www.sciencemag.org/content/356/6342/1081/suppl/DC1

Supplementary Material for

PCGF3/5–PRC1 initiates Polycomb recruitment in X chromosome inactivation

Mafalda Almeida, Greta Pintacuda, Osamu Masui, Yoko Koseki, Michal Gdula, Andrea Cerase, David Brown, Arne Mould, Cassandravictoria Innocent, Manabu Nakayama, Lothar Schermelleh, Tatyana B. Nesterova, Haruhiko Koseki, Neil Brockdorff*

*Corresponding author. Email: neil.brockdorff@bioch.ox.ac.uk

Published 9 June 2017, *Science* **356**, 1081 (2017)
DOI: 10.1126/science.aal2512

This PDF file includes:

Other Supplementary Material for this manuscript includes the following:
(available at www.sciencemag.org/content/356/6342/1081/suppl/DC1)

Materials and Methods

Plasmids

Coding sequences for PCGF1,2,3,5 and 6 proteins were amplified from cDNA prepared from 129/1 WT cell line using primers in Table S1. These sequences were inserted by LIC cloning into a modified pCAG-IRES-Puro mammalian expression plasmid between the coding sequence for a N-terminal enhanced GFP (eGFP) and a 3' IRES sequence that precedes Puromycin resistant gene. Similar plasmids were generated by inserting PCGF3 and 5 into a pCAG-IRES-Neo mammalian expression plasmid. RYBP coding sequence was obtained from cDNA prepared from 129/1 WT cell line using primers indicated in Table S1. The RYBP sequence was mutagenized into RYBP TF-AA using QuikChange Lightning Site-Directed Mutagenesis Kit (Agilent Genomics) according to manufacturer instructions and primers listed in Table S1. RYBP and RYBP TF-AA sequences were inserted by LIC cloning into a modified pCAG-IRES-Blast mammalian expression plasmid between the coding sequence for a N-terminal mCherry and a 3' IRES sequence that precedes the Blasticidin resistance gene.

Mouse lines and ESC lines derivation

M1 ES cells were derived from the cross between C57BL/6JJcl and 129^{+Ter}/SvJcl and used to produce a conditional knockout allele for *Pcgf1, Pcgf3* and *Pcgf5*. The arms of homology in targeting vectors span 2936 bp for 5' and 3260 bp for 3' of *Pcgf1*, 3051 bp for 5' and 3608 bp for 3' of *Pcgf3*, and 3018 bp for 5' and 3506 bp for 3' of *Pcgf5*, respectively. For *Pcgf1*, a Neomycin resistance gene flanked with FRT and loxP sequences was inserted at intron 7 and a loxP sequence at intron 1. For *Pcgf3*, a Neomycin resistance gene flanked with FRT and loxP sequences was inserted at intron 4 and a loxP sequence at intron 3. For *Pcgf5*, a Neomycin resistance gene flanked with FRT and loxP sequences was inserted at intron 2 and a loxP sequence at intron 1. To establish $Pcgf1^{fl/fl}$, $Pcgf3^{fl/fl}$ and $Pcgf5^{fl/fl}$ mouse lines, targeted ES cells were injected into mouse 8-cell stage embryos to create chimeric mouse lines, then those chimeric mice lines were mated with B6;SJL-Tg(ACTFLPe)9205Dym/J mice (The Jackson Laboratory) to remove the Neomycin resistance gene cassette. ES cell lines harboring the *Gt(ROSA)26Sor:CreERT2* allele were derived from matings between $Pcgf1^{fl/fl}$ and $Pcgf3^{fl/fl}$ lines and *Gt(ROSA)26Sor:CreERT2* line that was purchased from Artemis Pharmaceuticals (*21*). $Pcgf3^{+/-}$ and $Pcgf5^{+/-}$ mice used in crosses were derived by mating between $Pcgf3^{+/fl}$ and $Pcgf5^{+/fl}$ lines and CAG-Cre line (*22*).

ESC cell lines

Cell lines used in this study were 3E (*16*), 3E-H (derivative of 3E with Puromycin resistance cassette exchanged by a Hygromycin resistance cassette) (*18*), $Pcgf1^{fl/fl}$, $Pcgf3^{fl/fl}$ (derived for this study), $Ring1A^{-/-}$ $Ring1B^{fl/fl}$ (*23*), $Suz12^{-/-}$ *(14)* and mESCs with rtTA integrated into the *Gt(ROSA)26Sor* locus (cell line ACDI derived in house).

All ES cells were grown and passaged in feeder-dependent conditions on gelatinized plates with ESC medium at 37° C in a 5% CO_2 incubator. Mitomycin-inactivated SNLP (STO mouse fibroblasts expressing Neomycin, Puromycin resistance and *Lif* genes) were used as feeders. ESC medium consists of DMEM without sodium pyruvate (ThermoFisher) supplemented with 10% Fetal Calf Serum (Seralab), 1x non-essential amino acids (ThermoFisher), 2mM L-glutamine (ThermoFisher), 50µM β-mercaptoethanol

(ThermoFisher), 1x Penicillin-Streptomycin (ThermoFisher) and 1mL of Leukemia Inhibitory Factor-conditioned medium made in-house.

Xist expression driven by the TetO promoter was induced by adding doxycycline (1 to 1.5 μg/mL) to the culture medium for 6 h to 3 days depending on the experiment.

To ablate ubiquitylation from 3E mESCs, cells were treated with the reversible proteasome inhibitor MG132 (10μM) for 6 h before the experiment as previously described (*9*).

Conditional deletion of *Ring1B*, *Pcgf1* and *Pcgf3* was carried out by adding 800nM 4-hydroxytamoxifen to the culture medium for 48 h. To generate $Pcgf3^{-/-}$ $Pcgf5^{-/-}$ (constitutive knockout), cells were treated with 800nM 4-hydroxytamoxifen for 96 h.

Generation of stable cell lines expressing transgenes

All ES cells expressing transgenes in this study are stable expressing cell lines. To generate stable ES cell lines, cells were plated in 6-well plates on feeders at a density of 1-2x10^6 cells/well, a day before transfection. Medium was replaced with antibiotic-free medium before transfection. Cells were transfected using Lipofectamine 2000 (ThermoFisher), according to the manufacturer's instructions. After 24 h, transfected cells were passaged to gelatinized 90mm Petri dishes with feeders. Puromycin (1.5 to 2.5μg/mL), G418 (500 μg/mL) or Blasticidin (10μg/mL) selection was applied 48 h after lipofection. Cells were grown for 10-12 days under selection with medium being changed every day. Individual ES colonies were picked and expanded for screening. In all experiments at least two independent integrants were analyzed.

Targeting of rtTA-H cassette into *Gt(ROSA)26Sor* locus and screening by Southern blot

A modified version of pR26/P'nlsrtTA construct where the Puromycin resistance cassette was replaced by a Hygromycin resistance cassette (rtTA-H) (*18*) was electroporated into $Pcgf1^{fl/fl}$, $Pcgf3^{fl/fl}$ and $Ring1A^{-/-}$ $Ring1B^{fl/fl}$ to target rtTA-H into the constitutively active *Gt(ROSA)26Sor* locus as previously described *(16)*. Targeting was verified by Southern blot analysis using unique sequence probe as shown in Fig S1A.

Knockout of *Rybp*, *Yaf2* and *Pcgf5* using CRISPR/Cas9 mutagenesis

sgRNAs targeting *Rybp* and *Yaf2* were cloned into plasmid pX459. 3E-H mouse ES cells were plated in feeder-dependent conditions on a 6-well plate a day before transfection. On the day of transfection, medium was replaced with antibiotic-free medium. Cells in each well were transfected with 2μg of each plasmid using Lipofectamine 2000 (ThermoFisher), according to manufacturer's instructions. Cells were plated at different densities in three Petri dishes with feeders, 24 h after transfection. A day after, medium was replaced by ES medium with Puromycin (2μg/mL) for 48 h, after which cells were grown in ES medium until ES colonies were ready to be picked. Screening of knockout clones was achieved by Western blot or PCR from genomic DNA when the first was not possible. The clone selected for experiments was characterized using PCR followed by sequencing of the PCR product. sgRNAs targeting *Pcgf5* were cloned into plasmid pX462 *(24)* and transfected into $Pcgf3^{fl/fl}$ rtTA-H. The strategy used to produce and screen this cell line was similar to that described for *Rybp*/*Yaf2*.

Generation of *Xist* inducible clones

Pcgf1$^{fl/fl}$, *Pcgf3*$^{fl/fl}$ and *Pcgf3*$^{fl/fl}$ *Pcgf5*$^{-/-}$ ES cells with rtTA-H were co-transfected with an Xist plasmid containing a tandem array of 18 repeats of Bgl stem loop motif and a plasmid containing the fusion between the N-terminal RNA recognition motif of BglG and mCherry protein together with a neomycin resistance cassette as described (*18*). Stable cell lines were established using selection with 400 µg/mL G418 and screened by RNA-FISH for the presence of a single Xist cloud after doxycycline induction. Immunofluorescence against mCherry was used to identify clones with tagged Xist after 24 h of doxycycline treatment.

To establish an inducible Xist transgenic cell line, *Ring1A*$^{-/-}$ *Ring1B*$^{fl/fl}$ carrying a rtTA-H targeted into *Gt(ROSA)26Sor* locus was cotransfected with pTREXist vector *(16)* and a PGKpuro cassette. Cells were selected using 1.5 µg/mL Puromycin until individual ES colonies were picked. Colonies were screened by RNA-FISH for the presence of a single Xist cloud after doxycycline induction for 24 h. Xist deletion lines (ΔSX and ΔXN) and full length controls used constructs as described (*25*) and correspond to deletion of the A-repeats or F, B and partial C-repeats respectively. Stable autosomal integrants were made in male ESCs that had rtTA-H previously targeted into *Gt(ROSA)26Sor* locus as described above and screened by RNA-FISH for the presence of a single Xist cloud upon doxycycline induction.

Live cell imaging

Cells were plated on gelatinized µ-Slide 8 well slides or 35mm µ-Dishes (Ibidi), a day before Xist induction by doxycycline. Before imaging, cells were carefully washed with PBS and phenol red-free medium (Lonza) containing 2mM sodium pyruvate (ThermoFisher) and 12.5mM HEPES (ThermoFisher) was added. Live cell imaging was performed on an IX81 Olympus microscope connected to a Spinning Disk Confocal system (UltraView VoX PerkinElmer) equipped with an EMCCD camera (ImagEM, Hamamatsu Photonics) in a 25^{o} C heated chamber. All the pictures and z-stack movies were captured using a PlanApo 60x/ 1.4 N.A. oil-immersion objective heated to 37^{o} C, using Volocity 6.3 software (PerkinElmer). Images were captured with a 100ms exposure at 10% laser power and a detector sensitivity of 201. Z-stacks were captured every 0.8µm. All captured images were analyzed and processed using Fiji software.

FRAP and FRAP analysis

Fluorescence Recovery After Photobleaching (FRAP) was performed in the same setup described for live cell imaging. Photobleaching of a 1.25µm radius spot was performed by one bleach pulse of 50ms using 488nm laser at 100% intensity. Bleaching occurred after acquisition of 100 pre-bleach images. After bleaching, 500 images were captured at a maximum speed rate (approximately 8fps). Each image was captured with a 100ms exposure using 15% laser power and a detector sensitivity of 201. Experiment was repeated in three different days for the same stable cell line.

Fluorescence recovery was calculated normalizing for fluorescence before bleaching, background intensity and fluorescence loss due to photobleaching (*26, 27*). To determine the half recovery time $t_{1/2}$ and the percentage of immobile fraction (1-*v*) under the described conditions, FRAP data for each cell was fit to the following biexponential equation:

$$FRAP(t)= v-Ae^{-t/c}-Be^{-t/d}$$

where *t* is time, *v* is the plateau of the FRAP curve and *A*,*B*,*c* and *d* are fitted parameters (*27*).

Immunofluorescence

Cells were plated on slides at least a day before the experiment. On the day of the experiment, cells on slides were washed with PBS and then fixed with 2% formaldehyde for 15 min followed by 5 min of permeabilization using 0.4% Triton X-100. Cells were briefly washed with PBS before blocking with a 0.2% PBS-based solution of fish gelatin for three periods of 5 min. Primary antibody dilutions were prepared in fish gelatin solution with 5% normal goat or normal donkey serum depending on the secondary antibodies used. Primary antibody dilutions are listed in Table S2. Cells on slides were incubated with primary antibody for 1-2 h in a humid chamber at room temperature. Slides were washed three times in fish gelatin solution. Secondary antibodies were diluted 1:400 in fish gelatin solution and incubated with cells on slides for 1.5 h in a humid chamber at room temperature. After incubation, slides were washed twice with fish gelatin and one time with PBS before mounting using Vectashield mounting medium (Vector Labs) with 4′,6-diamidino-2-phenylindole (DAPI). Excess of mounting medium was removed and the coverslips were sealed to slides using nail varnish.

For the protocol using permeabilization before fixation, cells were plated in 6-well plates. On the day of the experiment, cells were washed with PBS, trypsinized and counted. Tubes containing $5x10^5$ cells were prepared and these cells were permeabilized by resuspension in 1mL of 0.4% Triton X-100 for 5 min. After 5 min 1mL of 4% formaldehyde solution was added to fix cells (in a final solution of 2% formaldehyde) for 15 mins. Cells were then cytospun onto slides. Slides were washed with PBS. Blocking, staining and mounting were performed as previously described.

Cells were analyzed on an inverted fluorescence Axio Observer Z.1 microscope using a PlanApo 63x/1.4 N.A. oil-immersion objective. Images were acquired using AxioVision software. Best exposure time for each field and channel was automatically determined by the software. A minimum of 100 cells was scored per slide and each experiment was scored in a minimum of 3 replicates.

Comparison of the size of H3K27me3 and H2AK119u1 domains between wild-type and *Rybp*$^{-/-}$ *Yaf2*$^{-/-}$ cells was performed using an in-house ImageJ (http://rsbweb.nih.gov/ij) pipeline on cells co-stained with both marks, and based on the manual identification and subsequent quantification of visible domains of signal enrichment. Technical replicates were obtained using alternative secondary antibodies.

For whole mount IF E7.5 embryos were obtained by IVF of *Pcgf3*$^{fl/fl}$*:Pcgf5*$^{fl/fl}$ oocytes with *Pcgf3*$^{fl/fl}$*:Pcgf5*$^{fl/fl}$:Cre-ERT2$^{+/-}$ sperm. To induce deletion of *Pcgf3/5* alleles two-cell embryos were treated with 4-hydroxytamoxifen (7.7µM) for 24h and transplanted into foster mothers. E7.5 embryos were dissected from uteri, rinsed in PBS containing 0.2% Tween-20 (PBS/Tween) and fixed in 2% formaldehyde/Tween for 15min at RT followed by 5 min quench in 200mM glycine/Tween. All following steps were essentially the same as for the cells, with the exception that all solutions were supplemented with 0.2% Tween-20. Images were acquired on Olympus FV1000 Laser Scanning Microscope.

Immuno-FISH

RNA FISH was performed essentially as described (*18*). Cells grown on slides were washed in PBS, and fixed with 4% formaldehyde for 10 min before permeabilisation in 0.4% Triton X-100 for 5 min. After washing in PBS, slides were incubated with 50% formamide in 2x SSC for 2 h. RNA probe was generated from an 18 kb fragment spanning the whole Xist transcript using a nick translation kit (Abbott Molecular) as previously described (*18*). Labelled RNA probe (1.5 µl) was co-precipitated with 10 µg salmon sperm DNA, 1/10

volume 3 M sodium acetate (pH 5.2) and 3 volumes ethanol. After washing in 75% ethanol, the pellet was dried, resuspended in 6 µl formamide and denatured at 75° C for 7 min before flash cooling on ice. Probe was diluted in 6 µl 2x hybridisation buffer (5x SSC, 12.5% dextran sulfate, 2.5 mg/ml BSA (NEB)), added to the slide and incubated overnight at 37° C in a humid chamber. Washes were performed twice in 50% formamide in 2x SSC for 3 min at 42° C, twice in 2x SSC for 3 min at 42° C and twice in PBS at room temperature. Slides were blocked in 0.2% fish gelatin (Sigma) three times for 2 min each, and primary antibodies were added in 0.2% fish gelatin and 5% normal goat serum in PBS. The slides were then processed in an identical manner to the immunofluorescence protocol detailed above.

Cells for super-resolution 3D-SIM were seeded onto No.1.5H (170 µm ± 5 µm) coverslips (Marienfield) and Xist expression was induced with doxycycline for 24h. Cells were fixed with 2% formaldehyde for 10 min, permeabilised in 0.5% Triton X-100 PBS for 10 min. Both initial blocking (30 min) and primary antibody incubation were carried out in 5% normal donkey serum (Santa Cruz) and 0.5% fish gelatin in PBS with 0.05% tween-20. Coverslips were incubated with primary antibody for 1 h in a humidified chamber (chicken anti-GFP, Abcam, ab13970). After extensive washing in PBS-T, coverslips were incubated with Goat anti-Chicken IgY (H+L) Alexa Fluor 488 (1/1000) for 45min at 37º C. Cells were again extensively washed, then post fixed with 2% formaldehyde. RNA-FISH was subsequently performed essentially as previously described, using 1 µg Xist cDNA labelled with red-dUTP (Abbott Molecular). Coverslips were incubated with 2 µg/ml DAPI for 10 min before mounting.

Structured Illumination Microscopy

Super-resolution 3D-SIM was performed on a DeltaVision OMX V3 Blaze system (GE Healthcare) equipped with a 60x/1.42 N.A. PlanApo oil immersion objective (Olympus), sCMOS cameras (PCO), and 405, 488 and 593nm lasers. 3D-SIM image stacks were acquired with a z-distance of 125nm and with 15 raw images per plane (5 phases, 3 angles). The raw data was computationally reconstructed with SoftWoRx 6.1 (GE Healthcare) using channel-specifically measured optical transfer functions (OTFs) and Wiener filter settings 0.0020 (green/red channel) and 0.0040 (blue channel), respectively, to generate 3D stacks with ~120 nm lateral and ~300 nm axial resolution. Spherical aberration was minimized by matching the refractive indices (RI) of the immersion oil for sample acquisition (RI 1.514) and for generation of OTFs (RI 1.512 for the blue and green, and 1.514 for the red OTFs) generated from ~170nm diameter blue PS-Speck beads (ThermoFisher) and 100 nm diameter green and red FluoSphere beads (ThermoFisher), respectively. Lateral color channel alignment was performed using a special image registration slide and algorithm provided by GE Healthcare. Correct 3D alignment was confirmed and refined in z by a custom test sample with two layers of 0.2µm diameter TetraSpeck beads (ThermoFisher). The full-scale 32-bit reconstructed data was thresholded for each channel to the stack modal grey value (representing the center of the background intensity level) and converted to 16-bit composite tif-stacks using an in-house script in ImageJ (http://rsbweb.nih.gov/ij) before further processing.

All 3D-SIM data was evaluated via *SIMcheck*, an open-source ImageJ plugin to assess SIM image quality (*28*) via modulation contrast-to-noise ratio (MCNR), spherical aberration mismatch (SAM), reconstructed Fourier plot (FTL; FTO) and reconstructed intensity histogram (RIH) values.

Nearest neighbor/minimal distance measurements were performed using a modified version of NNA, an Octave-executable script, available on GitHub [NNA (an Octave script) Copyright (C) 2014, 2015 Carnë Draug <carandraug+dev@gmail.com>]. Reconstructed and

aligned 3D-SIM data is thresholded to the modal intensity values, then converted to 16-bit. Nuclear (8-bit binary) masks were generated from the DAPI channel using a watershed algorithm to segment the signals from background, covering the entire nuclear space. After discarding connected components below 10 voxels in volume, sub-pixel centroid coordinates (x, y, z) falling within the DAPI mask are then assigned to each above-threshold call, allocated a unique identifier (an internal cross-reference structure paring all calls to its nearest neighbour in the partner channel) and exported to comma-separated-values format where appropriate statistical measures are subsequently applied.

RNA-FISH

For the experiment in *Ring1A*$^{-/-}$ *Ring1B*$^{fl/fl}$ ES cells, cells were plated on an extra slide in parallel with cells plated for immunofluorescence. After washing twice with PBS, cells were fixed for 10 min with 2.6% formaldehyde followed by permeabilization with 0.42% Triton X-100 for 5 min at 4^{o} C. After fixation, cells on slides were washed twice with 70% ethanol and dehydrated using a series of concentrated ethanol solutions (80%, 95% and 100%). Slides were briefly air dried before incubation with probe in a humid chamber overnight at 37^{o} C. Xist RNA probe was labeled and prepared as previously described for Immuno-FISH. After incubation, slides were washed three times with a solution of 2xSSC/50%formamide followed by three washes with 2xSSC in a water bath at 42^{o} C. Slides were mounted and sealed as for immunofluorescence.

Preparation of whole cell lysates and nuclear extracts

Total cell lysates were prepared from ES clones growing without feeders. Cells were washed with PBS and then lysed using Laemmli buffer (0.2M Tris pH 6.8, 2% SDS, 20% glycerol, 10% β-mercaptoethanol, 0.2% bromophenol blue). Cell lysates were snap frozen and kept at -20^{o} C until further use.

Nuclear extracts for immunoprecipitation and Western blot analyses of 3E-H expressing eGFP-PCGF proteins were prepared according to a modified version of the method described previously (*29*). Briefly, cells were lysed in buffer A (10mM HEPES pH 7.9, 1.5mM $MgCl_2$, 10mM KCl), incubated on ice for 10 min and recovered by centrifugation. Cells were then resuspended in 3 volumes of buffer A and nuclei were released using a Dounce homogenizer. Recovered nuclei were resuspended in buffer C (5 mM HEPES pH 7.9, 26% glycerol, 1.5 mM $MgCl_2$, 0.2 mM EDTA, 250 mM NaCl and complete protease inhibitors (Roche)). Salt concentration was increased to 400 mM NaCl and extraction was performed on ice for 1 h. Nuclei were pelleted at 13,000 rpm for 20 min at 4^{o} C and the supernatant was collected as nuclear extract. Samples concentration was measured using Bradford assay (Bio-Rad) according to manufacturers' instructions.

Immunoprecipitation

One milligram of nuclear extract (400 mM NaCl) was diluted into buffer C without NaCl to adjust to a final concentration of 150 mM NaCl in 1100 µl. All samples were treated with benzonase for 30 min rotating at 4 ^{o} C. After centrifugation to remove any precipitated protein, 100µl of the supernatant were collected as input. The remaining supernatant was transferred to a new protein LoBind tube (Eppendorf) and incubated with 1 µl of anti-GFP antibody (ab290, Abcam) rotating for 3 h at 4 ^{o} C. Protein A magnetic dynabeads (ThermoFisher) were pre-incubated with 1.5 mg/ml BSA for 2-3 h. 40 µl of beads were

added to each IP and incubated rotating for an extra 1 h at 4 ^{o} C. IP samples were washed five times in wash buffer (300 mM NaCl, 20 mM HEPES pH 7.9, 0.1% Tween-20, 5% glycerol) and then resuspended in 2x Laemmli Buffer and boiled for 10 min. Samples were stored at -20 ^{o} C until further analysis by Western blot.

Western blot

Total cell lysate and nuclear extract proteins were resolved on an SDS-PAGE separating gel with a stacking gel. After gel separation, proteins were transferred to a Hybond-P PVDF or nitrocellulose membrane (Amersham) using a semi-dry system (12V for 45 min or 17V for 1 h in the case of histones). Membranes were washed with PBS and then blocked for at least 1 h in blocking buffer (100 mM Tris pH7.5, 0.9% NaCl, 0.1% Tween, 5% non-fat milk) on a shaker at room temperature. Primary antibodies were prepared at the appropriate dilution in blocking buffer and membranes were incubated with antibody solutions overnight shaking at 4^{o} C. Antibody dilutions are indicated in Table S2. Membranes were washed 3 times 10 min each in blocking buffer and then incubated with secondary antibodies for an hour at room temperature. Secondary antibodies (either fluorescent-dye -1:15000- or horseradish peroxidase-conjugated antibodies -1:2000) were diluted in Blocking Buffer. After incubation, membranes were washed with blocking buffer twice, TBST (100mM Tris pH 7.5, 0.9% NaCl, 0.1% Tween) and PBS, 15 min each. The result was visualized either directly on ODYSSEY Fc Dual Mode Imaging System (LI-COR Biosciences Ltd, UK) for fluorescent-dye conjugated secondary antibodies or using enhanced chemiluminescence (ECL) solution for horseradish-peroxidase secondary antibodies.

Genotyping of mice and embryos

DNA for mice genotyping was obtained from their tail biopsies. DNA of E9.5 and E10.5 embryos was obtained from the yolk sac. E7.5 embryos were recovered after imaging and DNA was obtained from the entire embryos after overnight incubation with proteinase K. Genotyping PCR primers are listed in Table S1.

Xist Transgene mapping

Transgene mapping for *Pcgf3*$^{fl/fl}$*Pcgf5*$^{-/-}$ clone C3F8 was performed by the Chromosome Dynamics Core (Wellcome Trust Centre for Human Genetics, Oxford University). Briefly, Xist transgene plasmid used for generation of cells analyzed in this study was labeled by nick translation and hybridized together with a set of chromosome-specific probes onto the metaphase spreads isolated from mESCs. Transgene localization was confirmed by a FISH experiment using the probe for Xist transgene and RP23-290E4 BAC hybridizing in the pericentromeric region of chromosome 16 labeled with different fluorophores.

Chromatin RNA-Sequencing

Pcgf3$^{fl/fl}$*Pcgf5*$^{-/-}$ and *Pcgf3*$^{-/-}$*Pcgf5*$^{-/-}$ mESCs bearing Xist transgene on chromosome 16 (clone C3F8) were cultured in differentiating conditions (*16*): plated on non-gelatinized TC dish in ES medium without LIF for 72 h with (+dox) and without doxycycline (control). Cells were grown in parallel to confirm Xist induction by immunofluorescence using mCherry antibody as previously described.

RNA-Seq enriching for chromatin-bound nuclear RNA was performed according to a modified chromatin RNA-Seq protocol (*30*). The cells were spun down and re-suspended in 800 µl of hypotonic buffer HLBN (10 mM Tris-HCl pH 7.5, 10 mM NaCl, 2.5 mM $MgCl_2$, 0.05% NP40), under-layered with 480 µl of buffer HLBNS (HLBN, 12% sucrose). Nuclei were isolated by centrifuging for 5 min at 800 g. Supernatant containing the cytoplasmic fraction was discarded and the pellet containing nuclei was re-suspended in 100 µl of ice-cold buffer Nun1 (10 mM Tris-HCl pH 7.9, 75 mM NaCl, 0.5 mM EDTA, 50% glycerol, 1 mM DTT) supplemented with protease inhibitors (cOmplete EDTA free, Roche). Subsequently, 1200 µl of ice-cold buffer Nun2 (20 mM HEPES, 300 mM NaCl, 7.5 mM $MgCl_2$, 0.2 mM EDTA, 1 M urea, 1% NP40, 1 mM DTT) was added and the chromatin along with bound RNA was precipitated for 15 min on ice. Chromatin with RNA were pelleted by centrifuging at 14000 g and after discarding the nucleoplasmic fraction, re-suspended in 200 µl of buffer HSB (10 mM Tris-HCl pH 7.5, 500 mM NaCl, 10 mM $MgCl_2$,). After addition of 4U DNAse (TURBO DNAse, ThermoFisher), the DNA was digested for 10 min at 37º C while shaking at 1400 rpm on a ThermoMixer. Subsequently, 2 µl of 20% SDS and 4 µl of proteinase K (10 mg/ml, ThermoFisher, nuclease free) were added and the samples were incubated on a ThermoMixer for 30 minutes using the same settings as previously. Further the RNA was extracted using 1 ml of TRIzol (ThermoFisher Scientific) according to the manufacturer guidelines. RNA was dissolved in TURBO DNAse buffer, digested with TURBO DNAse for 30 min at 37º C on a ThermoMixer and extracted with TRIzol. RNA was washed three times with 75% ethanol, dissolved in water and quantified using a NanoDrop (ND-1000, ThermoFisher).

RNA quality was checked with RNA 6000 Pico Chip (Agilent Technologies) on Agilent 2100 Bioanalyser (Agilent Technologies). Samples were depleted of ribosomal RNA with Ribo-Zero Gold Kit (MRZG12324, Illumina) according to manufacturer's guidelines. RNA was isolated from 4 biological replicates.

RNA-Seq libraries were prepared with NEBNext® Ultra™ Directional RNA Library Prep Kit for Illumina (E7420S) using NEBNext® Multiplex Oligos for Illumina for multiplexing (E7335S and E7500S). Libraries were sequenced on NextSeq500 using NextSeq 500 High-Output Kit: 1 lane, 150 cycles, 75 bp paired end sequencing (Illumina).

Reads were mapped with STAR 2.5b aligner (*31*) to the mouse mm10 genome (GRCm38.p4 release) aided with mouse GTF file (gencode.vM12.annotation.gtf and dmel-all-r6.13.gtf files). Based on obtained bam files with reads aligned GTF file counts per gene were obtained with Htseq-count. Differential expression analysis was done with DESeq2, a package from the R Bioconductor project (*32)* using paired samples (+dox induced versus control cells) set up. Results were further processed, analyzed and visualized with custom R scripts using commonly used base and Bioconductor packages.

Table S1.
Oligonucleotides used in this study.

Cloning primer	Sequence (5'-3')
PCGF1_LIC_F	TACTTCCAATCCatgaggcttcggaaccagc
PCGF1_LIC_R	TATCCACCTTTACTGctacctcctcttctctttcac
PCGF2_LIC_F	TACTTCCAATCCatgcatcggaccacacgga
PCGF2_LIC_R	TATCCACCTTTACTGtcaaggggggcaaggagc
PCGF3_LIC_F	TACTTCCAATCCatgttgaccaggaagattaaac
PCGF3_LIC_R	TATCCACCTTTACTGtcaaggggggcaaggagc
PCGF5_LIC_F	TACTTCCAATCCatggctacccaaaggaaacac
PCGF5_LIC_R	TATCCACCTTTACTGctacccaaaatcaattctcggt
PCGF6_LIC_F	TACTTCCAATCCatggacgaggctgagacgg
PCGF6_LIC_R	TATCCACCTTTACTGtcaagttattttcaaaggagaaac
RYBP_LIC_F	TACTTCCAATCCaccatgaccatgggcgac
RYBP_LIC_R	TATCCACCTTTACTtcagaaagattcatcattc
Mutagenesis primer	**Sequence (5'-3'; mutations in capital and bold)**
RYBP_TF-AA_F	gattgtagcgtctgc**G**cc**GC**taggaacagcgccgaa
RYBP_TF-AA_R	ttcggcgctgttccta**GC**gg**C**gcagacgctacaatc
sgRNA target sequences	**Sequence (5'-3'; PAM sequence in bold)**
RYBP	CGCCCGGCAGGTACCTGGTC**GGG**
YAF2	GCCGAAGCCCGCCTCGGATG**AGG**
PCGF5_1	ATAGCCTTTACAGATGTAGC**AGG**
PCGF5_2	GATCAAGCCCACGACAGTGA**CGG**
Genotype primer	**Sequence (5'-3')**
CRE-S	CTCGACCAGTTTAGTTACCC
CRE-AS	ACGACCAAGTGACAGCAATG
PCGF1_F1	GCTGGACTTGGACGCTTGCGC
PCGF1_F2	AGTAAGCCCATCATGTTACGG
PCGF1_R1	GTACCTAAGAGGGAGATGGGC
PCGF3_F1	ATAAGATGAGATGGGATGGGC
PCGF3_F2	GTTGGTCTGTCAGTCAAGCCG
PCGF3_R1	ACGCCTCCAGGTGATCCATAC
PCGF5_F1	TGTTTACAGAGAGGAAGCGCC
PCGF5_F2	GACCCTGAAGGAGTTGGCTCG
PCGF5_R1	TGGCCTTGGTACACATATAGC
RYBP_F	CCGGTCGTCGTCCTCTTATT
RYBP_R	CCCCGGGTCTCCATCTTAG
Uba1XA	TGGTCTGGACCCAAACGCTGTCCACA
Uba1XB	GGCAGCAGCCATCACATAATCCAGATG
YAF2_F	CGTGTCCGGTTGTGTCCT
YAF2_R	ACATCGCACATCATGCACTT

Table S2.

Antibodies used in this study.

Antibody	Raised in	Source	Reference/ Cat. No.	Dilution for IF	Dilution for WB
H2AK119u1	Rabbit	Cell Signaling	mAb #8240	1:500-1:2000	1:1000
H3K27me3	Mouse	Active Motif	61017	1:500 – 1:2000	1:1000
GFP	Chicken	Abcam	ab13970	1:500	-
GFP	Rabbit	Abcam	Ab290	-	1:1000
mCherry	Rabbit	Source BioScience	ABE3523	1:500	-
mCherry	Sheep	Gift from F. Barr	-	1:500	-
RING1B	Mouse	Gift from H. Koseki	-	-	1:3000
RYBP	Rabbit	Millipore	AB3637	-	1:500
PCGF1	Rabbit	Gift from R. Klose	-	-	1:500
CBX7	Rabbit	Abcam	ab21873	-	1:1000
EZH2	Rabbit	Cell Signaling	mAb #5246	1:500	1:1000
SUZ12	Rabbit	Cell Signaling	mAb #3737	-	1:1000
EED	Mouse	Gift from A. Otte	-	1:100	1:1000
Histone H3 (loading control)	Rabbit	Abcam	ab1791	-	1:1000
Histone H4 (loading control)	Rabbit	Abcam	ab7311	-	1:1000
Lamin B (loading control)	Goat	Santa Cruz	sc6216 and sc6217	-	1:1000
TBP (loading control)	Mouse	Abcam	ab51841	-	1:1000
Tubulin (loading control)	Rabbit	Cell Signaling	#2144	-	1:1000

Supplementary Text

Note S1

We engineered an inducible Xist transgene into mESCs with a conditional knockout allele of *Ring1B* on a *Ring1A* null background (*Ring1A*$^{-/-}$ *Ring1B*$^{fl/fl}$). The rtTA-H cassette was inserted into one allele of the *Gt(ROSA)26Sor* locus by homologous recombination (Fig S1A), with a Cre-ERT2 cassette being present on the other allele. Cells were then transfected with a Xist transgene driven by the TetO promoter. Within 48 h of tamoxifen treatment (+OHT) we observed depletion of RING1B protein and H2AK119u1, but no significant change in levels of PRC2 (EZH2) or H3K27me3 (Fig S1B).

Note S2

Using IF we were able to detect eGFP-PCGF3, eGFP-PCGF5, and to some extent eGFP-PCGF6 co-localising with H2AK119u1 domains, used as a proxy for the inactive chromosome (Fig S3E,F). eGFP-PCGF2 localisation was rarely detectable and eGFP-PCGF1 localisation not at all (Fig S3E,F). A prior study determined that highly dynamic interactions of a chromatin binding factor, MeCP2, are captured relatively inefficiently using formaldehyde cross-linking compared to live cell imaging (*33*). A threshold of $t_{1/2}$ >5s was determined as being required to efficiently detect protein enrichment by IF. Our FRAP measurements of eGFP-PCGF dynamics within Xist domains demonstrated fast dynamics (<5s) for the bulk of eGFP-PCGF proteins, except eGFP-PCGF3 and eGFP-PCGF5 for which there was a significant immobile fraction (Fig 2B, Fig S4B,D). We conclude that inefficient cross-linking likely accounts for our inability to detect H2AK119u1 domain enrichment of eGFP-PCGF complexes that have rapid chromatin binding dynamics.

Note S3

To compare the dynamics of eGFP-PCGF fusions, we calculated the rate of turnover ($t_{1/2}$) by fitting recovery curves with a bi-exponential equation (27). The distribution of $t_{1/2}$ values reflect the kinetics of the transient (<60s) fraction (Fig. S4C). For eGFP-PCGF1/2/3 turnover of the transient fraction within the Xist RNA domain is only marginally slower than bulk nucleoplasm. Slower turnover of eGFP-PCGF5/6 (~3-5s) may reflect an enrichment of binding sites within the Xist RNA domain, or the presence of distinct interactions not found in bulk nucleoplasm. Despite slower turnover of transiently bound eGFP-PCGF6 relative to eGFP-PCGF1/2/3 (Fig. S4C), the protein does not appear to form a stably bound fraction at the Xist RNA domain (Fig. S4D). Conversely eGFP-PCGF3 forms a stably bound fraction despite the relatively fast turnover of its transient interactions with the Xist RNA domain.

Note S4

We generated *Rybp*$^{-/-}$*Yaf2*$^{-/-}$ mESCs using CRISPR/Cas9 mediated mutagenesis in the 3E-H cell line carrying an inducible Xist transgene (Fig S5A). *Rybp*$^{-/-}$*Yaf2*$^{-/-}$ mESCs showed no gross change in global levels of H2AK119u1, H3K27me3, nor of core PRC1 and PRC2 subunits, as determined by western blot analysis (Fig S5B). We went on to generate *Rybp*$^{-/-}$ *Yaf2*$^{-/-}$ sublines stably expressing each of the eGFP-PCGF fusion proteins, and analysed

localisation to Xist RNA domains (Movies S2-S6) as described for experiments illustrated in Fig 2.

Note S5

We analysed the timecourse for H2AK119u1 and H3K27me3 deposition in response to Xist RNA expression both in 3E-H mESCs and in the derivative *Rybp*$^{-/-}$*Yaf2*$^{-/-}$ cell line, performing IF for both modifications at different timepoints between 0 and 24h of doxycycline treatment (Fig S5E). The appearance of domains was evident as early as 2 h after Xist induction. However, the rate of accumulation of H2AK119u1 domains was considerably more rapid than for H3K27me3. At 24 h both modifications were detectable as domains in a similar proportion of cells. These observations support the contention that H2AK119u1 precedes and is required for H3K27me3 deposition.

Note S6

We reasoned that an increase in the nucleoplasmic pool of unbound PRC1 complexes in *Rybp*$^{-/-}$*Yaf2*$^{-/-}$ mESCs may mask enrichment over Xist RNA domains. To test this we employed a modified IF protocol in which prior permeabilisation of cells was used to deplete the unbound pool prior to fixation. Under these conditions we were able to detect Xist RNA domain enrichment for eGFP-PCGF3 and eGFP-PCGF5, but not for the other eGFP-PCGF fusion proteins (Fig. S6B).

Note S7

For functional analysis of PCGF1 we engineered an inducible Xist transgene tagged with Bgl stem loops together with Bgl-mCherry into mESCs with conditional *Pcgf1* knockout alleles (*Pcgf1*$^{fl/fl}$) (Fig S7A-C). Similarly, we engineered an inducible Xist transgene into mESCs with a conditional *Pcgf3* knockout allele (*Pcgf3*$^{fl/fl}$) (Fig S7A,B,D). A *Pcgf5* null allele was generated by CRISPR/Cas9 mutagenesis in *Pcgf3*$^{fl/fl}$ mESCs (Fig S7E), either before or after integration of the inducible Xist transgene (Fig S7A), thus enabling analysis of the effects of deleting *Pcgf5* alone or together with *Pcgf3*.

Note S8

eGFP-PCGF3 and eGFP-PCGF5 expression constructs were transfected into an mESC line that has an inducible Xist transgene and in which the essential PRC2 subunit *Suz12* gene was mutagenised using the CRISPR/Cas9 technology. Live cell imaging results demonstrated that both eGFP-PCGF3 and eGFP-PCGF5 fusion proteins localise to Xist domains (Fig S9A), despite complete absence of PRC2/H3K27me3 *(14)*.

Note S9

eGFP-PCGF3 and eGFP-PCGF5 expression constructs were transfected into mESCs expressing either ΔSX or ΔXN Xist transgenes as described in Figure S2. Live cell imaging revealed both constructs are expressed (nuclear eGFP signal) but localization to Xist RNA domains occurs only in the ΔSX mESCs (Fig S9B). These results were confirmed by Immuno-FISH using GFP antibody and Xist RNA probe (Fig S9C). These observations confirm the requirement of the XN region for recruitment to PCGF3/5-PRC1 complexes by Xist RNA.

Note S10

3D-SIM super resolution microscopy was applied in order to determine the proximity of Xist RNA to the different non-canonical PRC1 complexes, based on Immuno-FISH detection of eGFP-PCGF fusion proteins and Xist RNA. eGFP-PCGF3/5 were consistently closer to Xist RNA than eGFP-PCGF1/2/6 (Fig S10B). The difference in average distance, approximately 50nm, is similar to that between hnRNPU/SAFA, which interacts directly with Xist RNA (*34*), and PRC2 subunits (*6*), which are recruited by binding to H2AK119u1 chromatin. The distances obtained for eGFP-RING1B were marginally less than for eGFP-PCGF1/2/6, consistent with the signal representing a median value for the different canonical and non-canonical PRC1 complexes.

Note S11

To obtain *Pcgf3*$^{-/-}$:*Pcgf5*$^{-/-}$ knockout embryos at E7.5, *Pcgf3*$^{fl/fl}$:*Pcgf5*$^{fl/fl}$ oocytes were in vitro fertilized with *Pcgf3*$^{fl/fl}$:*Pcgf5*$^{fl/fl}$:CreER$^{+/-}$ sperm. To induce deletion of *Pcgf3* and *Pcgf5* alleles two cell embryos were treated with 4-hydroxytamoxifen for 24 h and transplanted into foster mothers. Embryos were dissected from uteri at E7.5.

Note S12

From heterozygote crosses, E9.5 homozygous mutant male embryos appeared similar to wild-type, whereas at E10.5 they were often of reduced size. In female homozygous mutant conceptuses the embryos were extensively degraded at E9.5 and E10.5. Placentas were intact at E9.5 and in one case at E10.5 (Fig S12A). Histological analysis of the placentas from E9.5 *Pcgf3*$^{-/-}$:*Pcgf5*$^{-/-}$ embryos and matched controls, illustrated in Fig S12B, revealed that males have some parietal trophoblast giant cells (TGCs), but fail to form a labyrinth, despite the presence of chorionic trophoblasts in two of three samples. The phenotype of the female double homozygous mutant placentas is more striking since they essentially lack trophoblasts altogether, and as a consequence fail to form a labyrinth.

Note S13

For RNA-Seq analysis we used the chromatin RNA-Seq method to enrich for nascent transcripts *(30)*. Analysis was performed in quadruplicate using *Pcgf3*$^{fl/fl}$ *Pcgf5*$^{-/-}$ mESCs (no effect on Xist mediated recruitment of Polycomb complexes), comparing with *Pcgf3*$^{-/-}$*Pcgf5*$^{-/-}$ mESCs (no detectable Polycomb recruitment) derived therefrom (Fig 4C). The Xist transgene was mapped to mouse chromosome 16 (Fig S13A). Applying stringent parameters (FDR 0.1) to identify genes with different expression levels following induction of Xist expression for 72 h, we found that chromosome 16 had the highest number of differentially expressed genes, most of which were downregulated (Fig S13B). This contrasts with other chromosomes (chromosome 15 and 17), where the proportion of upregulated and downregulated genes was in most cases very similar (Fig S13B-D). The number of downregulated genes on chromosome 16 was significantly reduced in the *Pcgf3*$^{-/-}$ *Pcgf5*$^{-/-}$ mESCs compared to *Pcgf3*$^{fl/fl}$ *Pcgf5*$^{-/-}$ mESCs (14 compared to 91 genes) (Fig 4E, Additional Data Table S1).

Fig S1

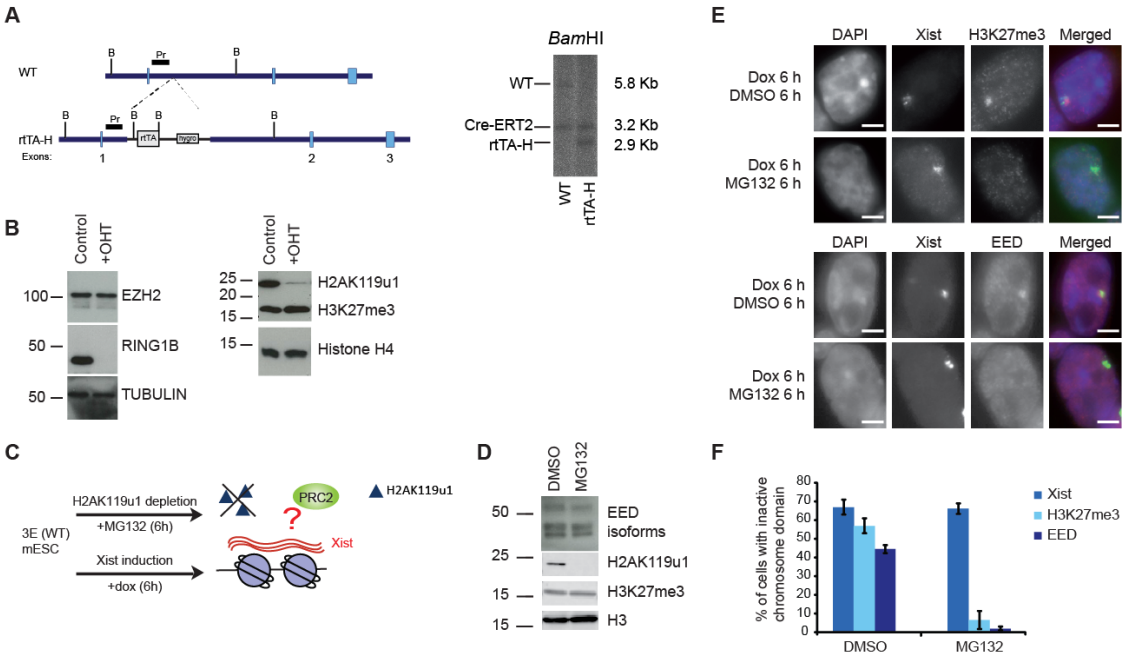

Fig. S1 H2AK119u1 mediates PRC2 recruitment by Xist RNA.

(A) Targeting strategy and Southern blot illustrating targeting of rtTA-H into the *Gt(ROSA)26Sor* locus in *Ring1A*$^{-/-}$ *Ring1B*$^{fl/fl}$ mESCs. (B) Western blots of Polycomb proteins (EZH2 and RING1B), and Polycomb mediated histone modifications (H2AK119u1 and H3K27me3), before and 48 h after tamoxifen (+OHT) addition for Cre-ERT2 mediated deletion of *Ring1B*. Loading controls are Tubulin and histone H4. (C) Schematic representation of the experiment. Xist transgene expression is induced for 6 h in the presence of MG132, which depletes H2AK119u1 in 3E mESCs. (D) Western blot analysis illustrating global levels of the PRC2 subunit EED and the histone modifications H2AK119u1 and H3K27me3 in 3E mESCs treated with DMSO or treated with MG132 for 6 h. Loading control is histone H3. (E) Immuno-FISH for Xist RNA and EED protein in mESCs with an induced inactive chromosome after 6 h of DMSO or MG132 treatment. Scale bar is 5 µm. (F) Bar chart represents percentage of cells with domains for Xist, H3K27me3 and EED in DMSO and MG132 treated cells after Xist induction for 6 h. A minimum of 300 cells were counted in 3 biological repeats. Error bars indicate standard deviation.

Fig S2

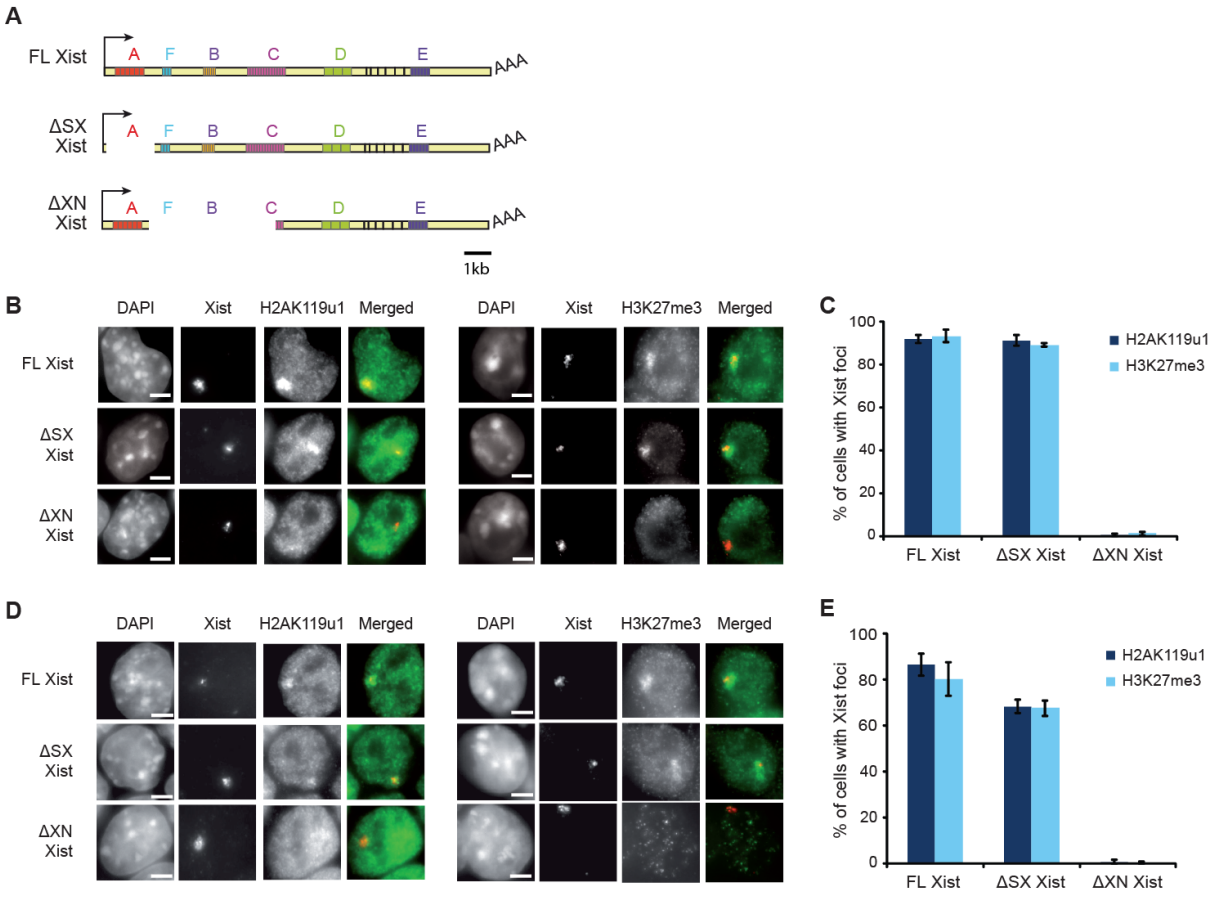

Fig. S2 Xist XN region mediates recruitment of PRC1 and PRC2.

(A) Diagram of full length Xist cDNA and deletion constructs. ΔSX removes the A-repeat, ΔXN removes the F-, B- and some of the C-repeats. (B) Immuno-FISH experiment for Xist RNA and either H2AK119u1 (left panel) or H3K27me3 (right panel) after doxycycline induction of full length Xist transgenes or deletion constructs. Scale bar is 5 μm. (C) Bar chart represents percentage of cells with domains for H2AK119u1 or H3K27me3 overlapping with Xist RNA foci observed in B. A minimum of 300 cells were counted in 3 biological repeats. Error bars indicate standard deviation. (D) Immuno-FISH experiment for Xist RNA and either H2AK119u1 (left panel) or H3K27me3 (right panel) after doxycycline induction of full length Xist transgenes or deletion constructs in independently derived mESC clones. Scale bar is 5 μm. (E) Bar chart represents percentage of cells with domains for H2AK119u1 or H3K27me3 overlapping with Xist RNA foci observed in D. A minimum of 300 cells were counted in 3 biological repeats. Error bars indicate standard deviation.

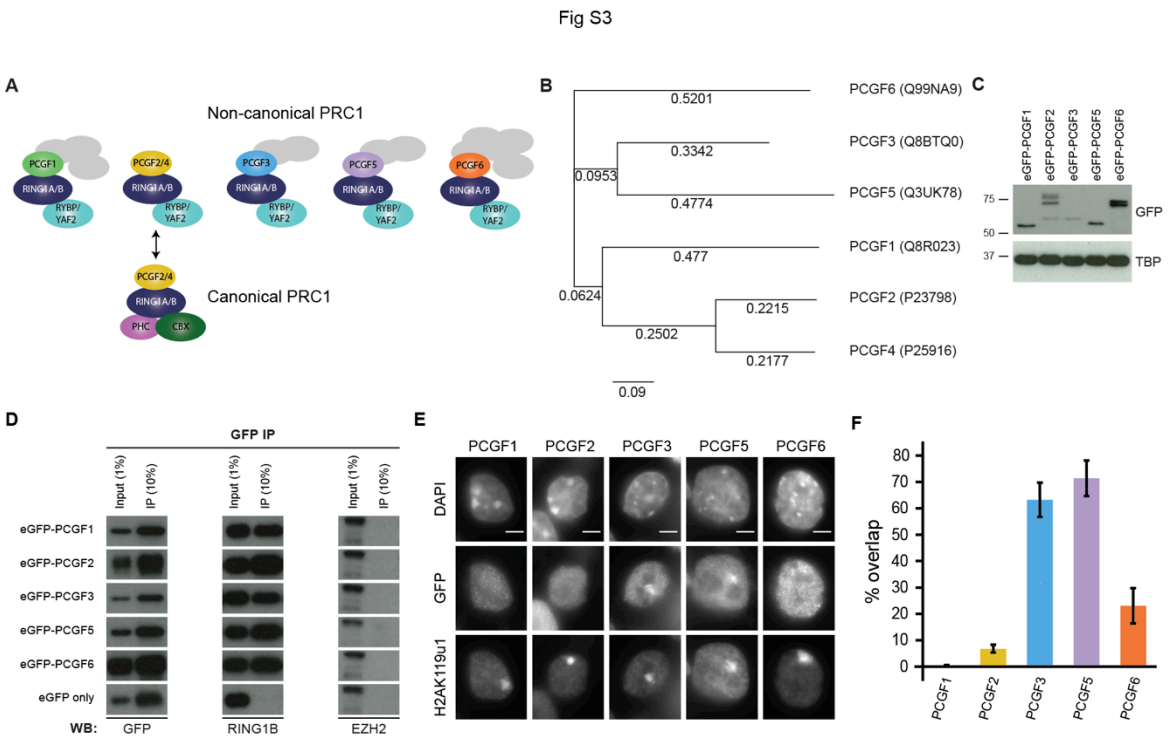

Fig. S3 Xist dependent localization of non-canonical PRC1 complexes.

(A) Schematics illustrating subunits of non-canonical and canonical PRC1 complexes. Grey ovals indicate additional subunits that are not discussed in this study. (B) Neighbor Joining phylogenetic tree of mouse PCGF amino acid sequences (UNIPROT ID in brackets). Numbers represent amino acid substitutions per site. (C) Western blot illustrating levels of eGFP-PCGF fusion proteins in stable cell lines in Fig. 2. TATA-binding protein (TBP) is used as loading control. (D) Western blot illustrating co-immunoprecipitation of endogenous RING1B with eGFP-PCGF fusion proteins using anti-GFP antibody and nuclear extracts from stable cell lines in Fig. 2. A stable cell line expressing eGFP only and EZH2 Western blot were used as negative controls for the co-immunoprecipitation experiment. (E) mESC lines in Fig. 2 analysed by IF following induction of Xist for 24 h. Images show representative single cells stained for GFP and H2AK119u1. DNA was counterstained with DAPI. Scale bar is 5 µm. (F) Bar chart represents percentage of cells in which focal localization of H2AK119u1 and eGFP-PCGF fusion proteins coincides (% overlap). Data was obtained from scoring a minimum of 400 cells in at least four replicates. Error bars indicate standard deviation between replicates.

Fig S4

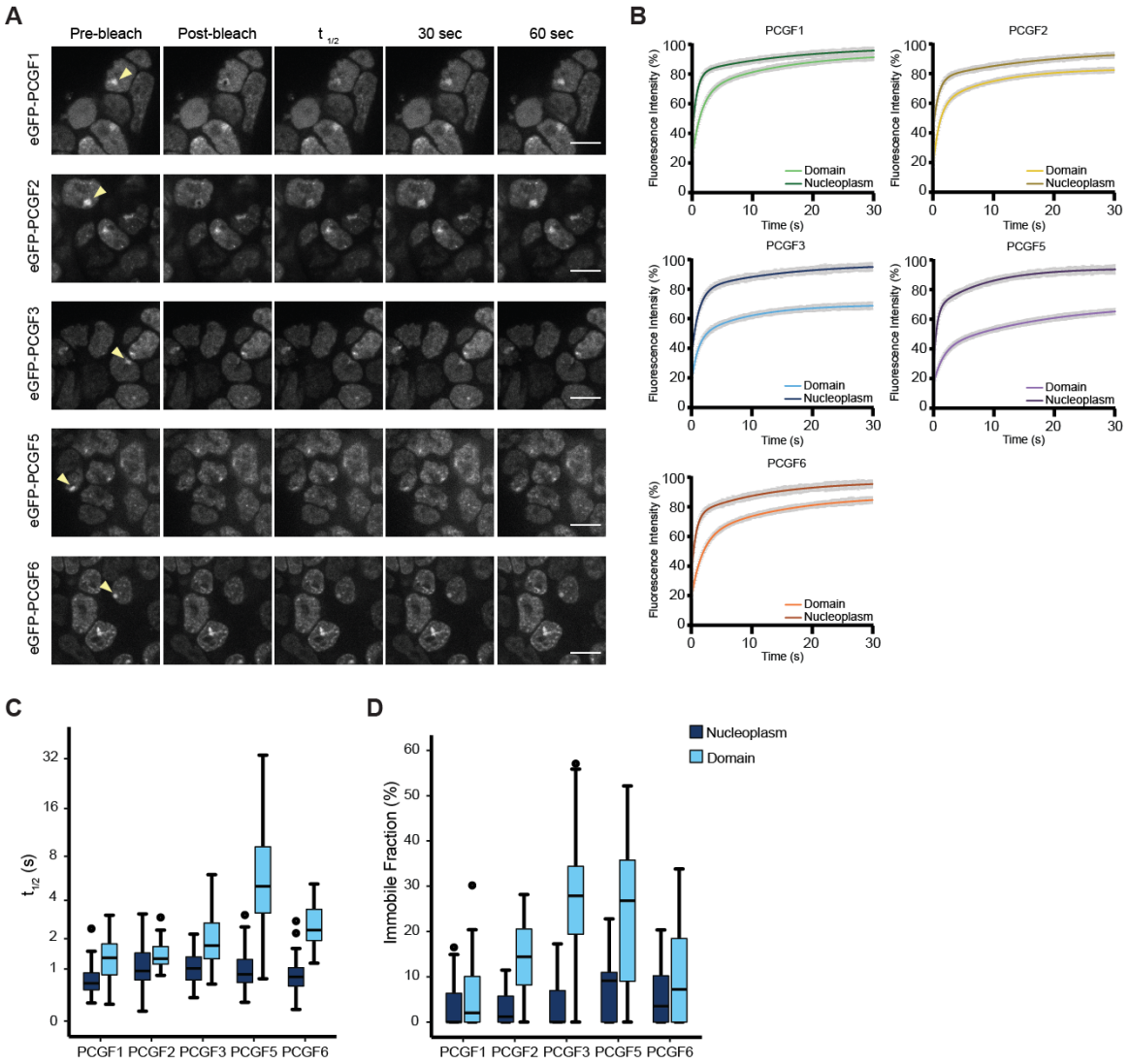

Fig. S4 Dynamic behavior of eGFP-PCGF fusion proteins.

(A) Maximum intensity projections of single frames showing examples of different timepoints during FRAP acquisition (Pre-bleach, first frame Post-bleach, time corresponding to recovery of half of the fluorescence [$t_{1/2}$], 30 s after bleaching and 60 s after bleaching) for different eGFP-PCGF expressing cell lines. Arrows highlight bleached domains. (B) Fitted FRAP curves are shown superimposed on plots of the standard error of the mean, illustrating the bi-exponential fit. Recovery curves are shown for domain and nucleoplasm for each eGFP-PCGF fusion protein as indicated. (C) Distribution of the rate of turnover ($t_{1/2}$) for eGFP-PCGF fusion proteins calculated for the nucleoplasm and Xist RNA domains. $t_{1/2}$ is shown in seconds and represented on a log2 scale. (D) Distribution of the percentage of eGFP-PCGF fusion proteins in the immobile fraction calculated for nucleoplasm and Xist RNA domains.

Fig S5

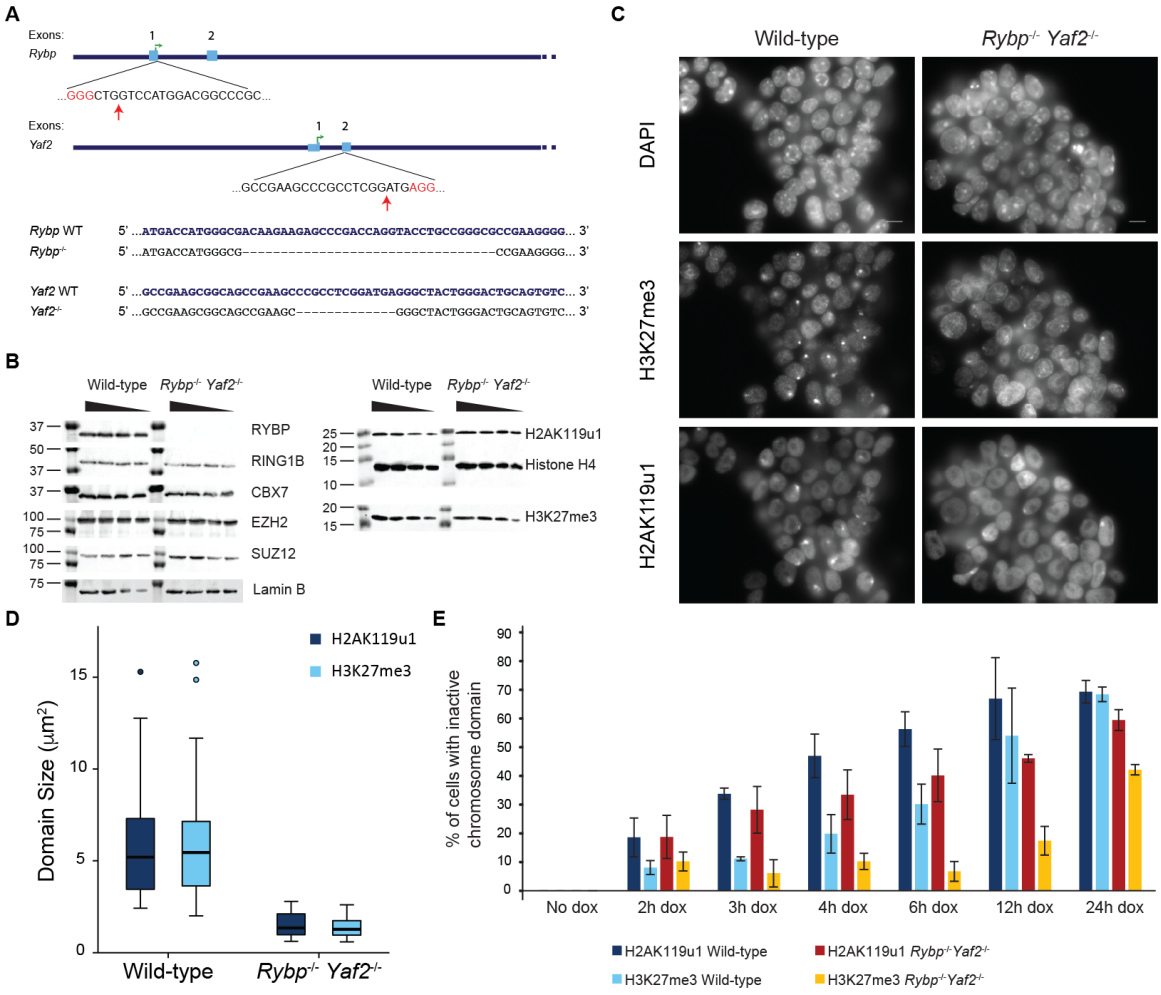

Fig. S5 Generation and characterisation of *Rybp*$^{-/-}$ *Yaf2*$^{-/-}$ mESC line.

(A) Strategy for CRISPR-Cas9 mediated mutagenesis of *Rybp* and *Yaf2* genes. The position of guide RNAs relative to *Rybp* and *Yaf2* is shown, with PAM sequences (red font) and predicted cleavage sites (red arrows) indicated. An alignment of wild-type sequence with frameshift deletions of the clone used in this study is shown below. (B) Western blot analysis of the PRC1 subunits RYBP, RING1B, and CBX7, the PRC2 subunits EZH2 and SUZ12, and the histone modifications H2AK119u1 and H3K27me3 in *Rybp*$^{-/-}$ *Yaf2*$^{-/-}$ compared to wild-type mESCs. Lamin B and histone H4 western blots are included as loading controls. Volumes loaded were 14 µl, 10 µl, 8 µl and 6 µl (WCE) or 10 µL, 7 µL, 5 µL and 2 µL (histone extract). Molecular weight markers are shown on the left. (C) Immunofluorescence analysis of H3K27me3 and H2AK119u1 domains in *Rybp*$^{-/-}$ *Yaf2*$^{-/-}$ mESCs compared to wild-type mESCs. Images show a representative mESC colony after 24h of Xist induction. Scale bar is 5 µm. (D) Boxplot showing quantification of the domain size for H2AK119u1 and H3K27me3 in *Rybp*$^{-/-}$ *Yaf2*$^{-/-}$ mESCs compared to wild-type mESCs after 24 h of Xist induction. (E) Bar chart represents percentage of cells showing H2AK119u1 and H3K27me3 domains at different time-points after Xist induction (+dox) in wild-type and *Rybp*$^{-/-}$ *Yaf2*$^{-/-}$ mESC lines. Data was obtained from scoring a minimum of 300 cells in at least three replicates. Error bars indicate standard deviation between replicates.

Fig S6

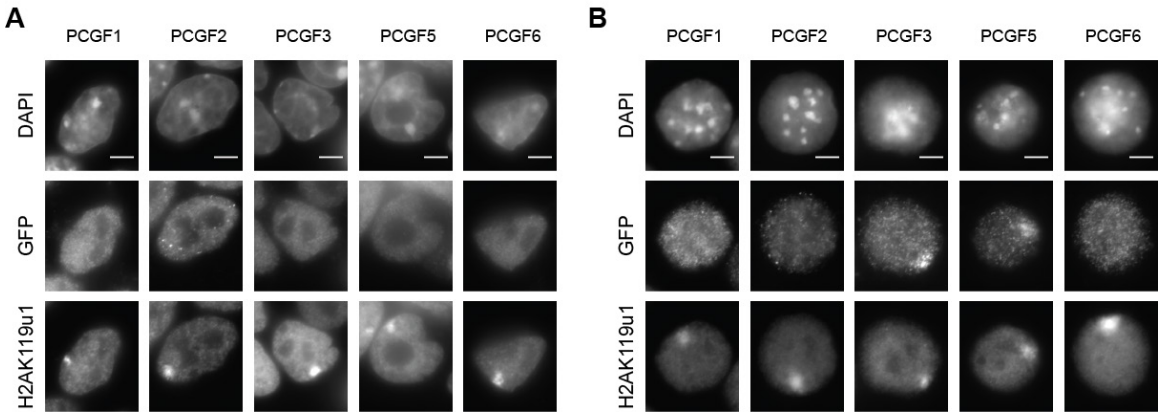

Fig. S6 Immunofluorescence analysis of eGFP-PCGF localization to the inactive chromosome domain in *Rybp*$^{-/-}$ *Yaf2*$^{-/-}$ mESC line.

(A) Immunofluorescence analysis of *Rybp*$^{-/-}$ *Yaf2*$^{-/-}$ cells expressing eGFP-PCGF fusion proteins. Images show representative single cells stained for GFP and H2AK119u1 in conventional fix/perm conditions. Scale bar is 5 μm. (B) Immunofluorescence analysis of *Rybp*$^{-/-}$ *Yaf2*$^{-/-}$ mESCs expressing eGFP-PCGF fusion proteins. Images show representative single cells stained for GFP and H2AK119u1 in perm/fix conditions. Scale bar is 5 μm.

Fig S7

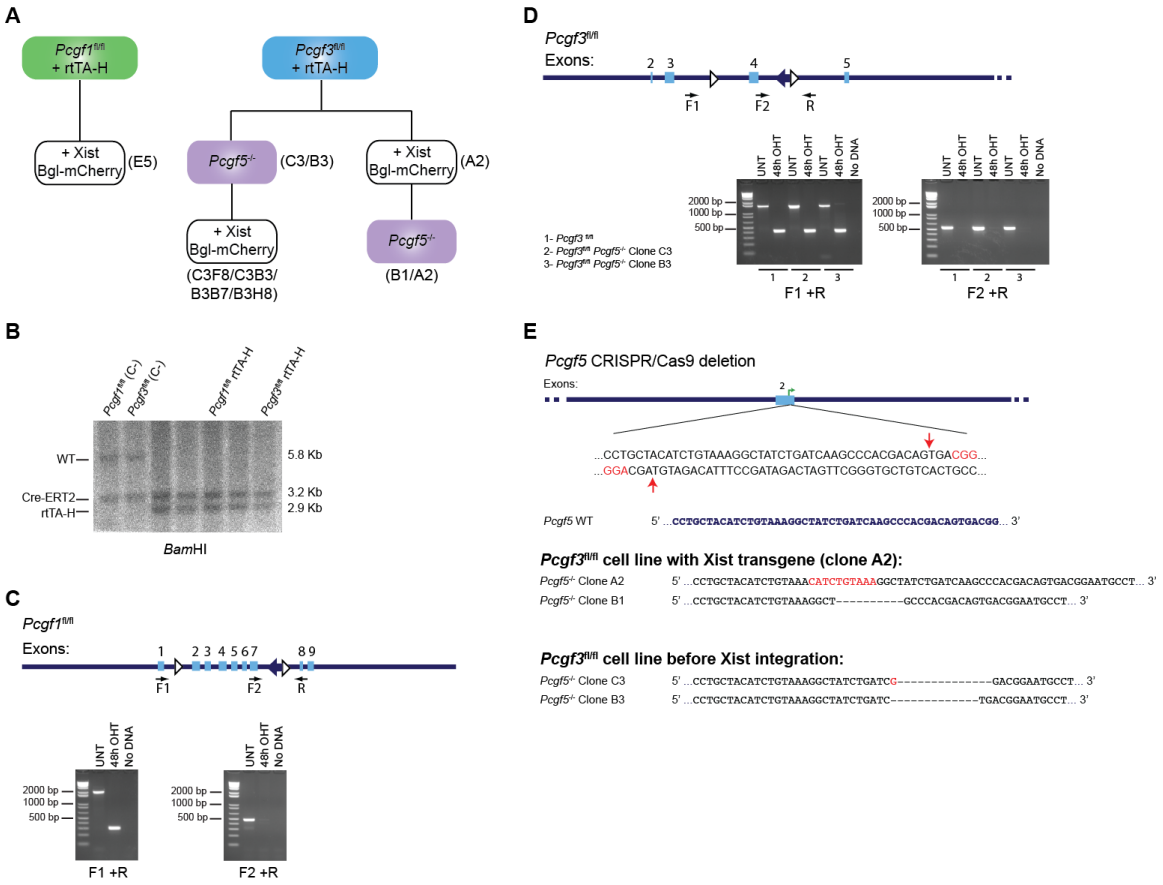

Fig. S7 Engineering of conditional and constitutive *Pcgf* knockout mouse ESCs and targeting of rtTA-H cassette into *Gt(ROSA)26Sor* locus.

(A) Schematic of knockout mESC lines with inducible Xist Bgl-mCherry system used in this study. Clones selected for each cell line are shown in brackets. (B) Gene targeting of rtTA-H cassette into the *Rosa26* locus in *Pcgf1*$^{fl/fl}$ and *Pcgf3*$^{fl/fl}$ mESCs using the same strategy as in Fig S1A. Southern blot illustrating that parent mESC lines (C-) and rtTA-H lines have Cre-ERT2 integrated into one allele of the *Gt(ROSA)26Sor* locus and targeted clones have rtTA-H integrated into the second allele. (C) Strategy for conditional null allele of *Pcgf1* (*Pcgf1*$^{fl/fl}$). Schematics show intron/exon structure of the regions of interest with loxP (open triangles) and frt (filled triangle) site specific recombination recognition sites indicated. PCR primers used to discriminate floxed and deleted alleles are indicated (F1, F2 and R). PCR analysis illustrates deletion of *Pcgf1* after 48 h of tamoxifen treatment (48 h OHT) compared to untreated cells (UNT). (D) Strategy for conditional null alleles of *Pcgf3* (*Pcgf3*$^{fl/fl}$). PCR analysis illustrates deletion of *Pcgf3* in *Pcgf3*$^{fl/fl}$ mESCs and also in two independent clones, C3 and B3 in which *Pcgf5* was first deleted by CRISPR/Cas9 mediated mutagenesis. (E) Strategy for CRISPR/Cas9 mediated knockout of *Pcgf5* showing the location of guide RNA (PAM sequences in red) and predicted cleavage sites (red arrows). Sequence of the wild-type and all *Pcgf5* mutant mESC lines used in this study is shown below.

Fig S8

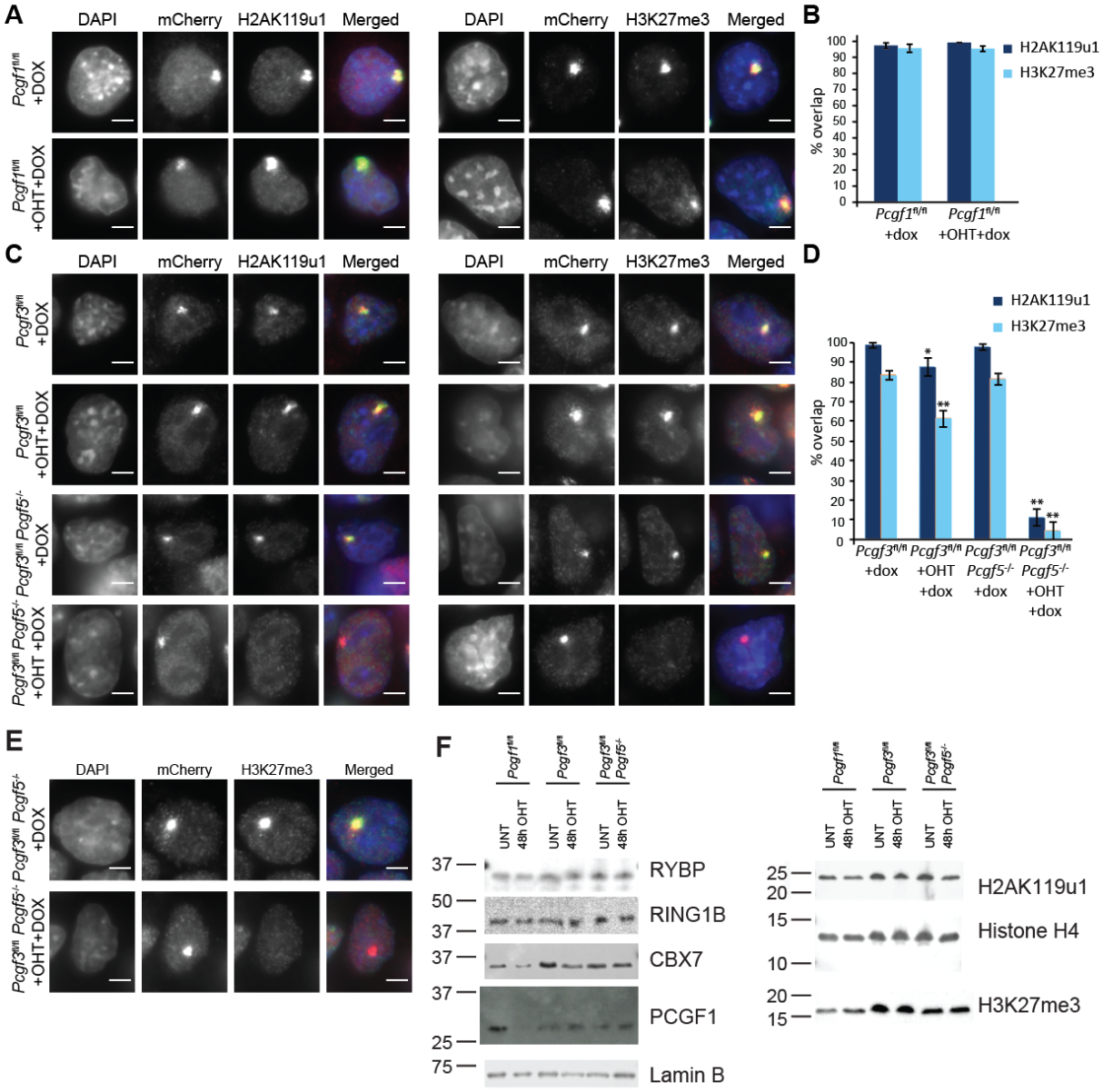

Fig. S8 Effect of *Pcgf1*, *Pcgf3*, *Pcgf5* and *Pcgf3/5* knockouts in Polycomb recruitment by Xist RNA.

(A) Immunofluorescence analysis of mCherry-Bgl Xist (mCherry) and H2AK119u1/H3K27me3 in the presence and absence of PCGF1. Scale bar is 5 µm. (B) Bar chart represents percentage of overlap of histone modification enrichment with mCherry domain. Scoring data was obtained from a minimum of 300 cells in three replicates. Error bars show standard deviation. (C) Immunofluorescence analysis of mCherry-Bgl Xist (mCherry) and H2AK119u1/H3K27me3 in the presence and absence of PCGF3, PCGF5 and both PCGF3 and PCGF5. Scale bar is 5 µm. (D) Bar chart represents percentage of overlap of histone modification enrichment with mCherry domain. Scoring data was obtained from a minimum of 300 cells in three replicates. Error bars show standard deviation. Significant differences relative to *Pcgf3*$^{fl/fl}$ +dox (Student t-test) are indicated (*p<0.01, **p<0.001). (E) Immunofluorescence analysis of mCherry-Bgl Xist (mCherry) and H3K27me3 in the presence and absence of PCGF3 in *Pcfg5*$^{-/-}$ mESCs corresponding to clones represented in Fig 4B,C. Scale bar is 5 µm. (F) Western blot analysis of PRC1 (RYBP, RING1B, CBX7)

subunits, and H3K27me3 and H2AK119u1 histone modifications, before (UNT) and after (48 h OHT) deletion of *Pcgf1*, *Pcgf3* or both *Pcgf3* and *Pcgf5*. Loading controls are Lamin B and histone H4.

Fig S9

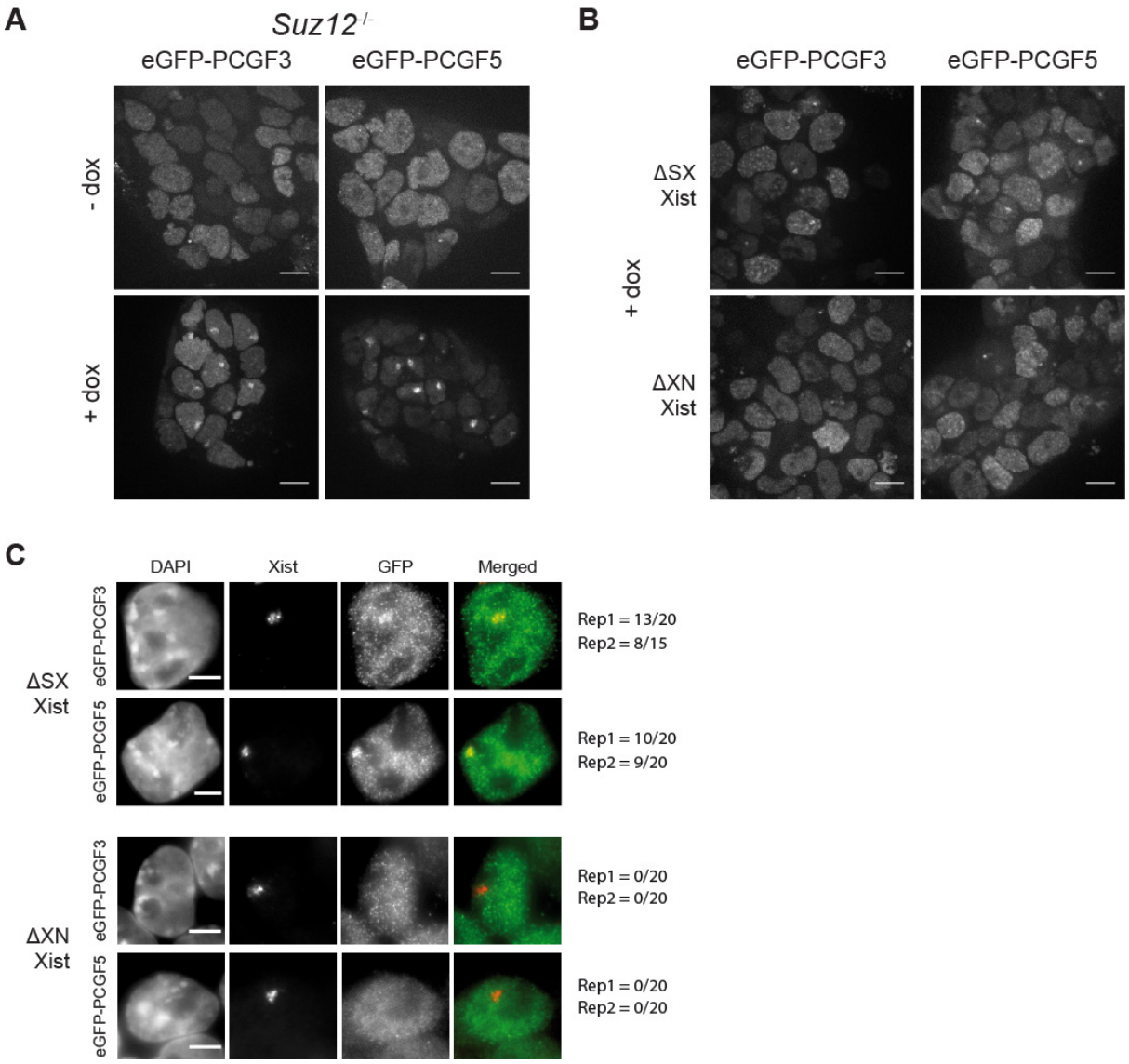

Fig. S9 eGFP-PCGF3 and eGFP-PCGF5 localization to the inactive chromosome depends on Xist XN region but not on PRC2 or Xist SX region.

(A) Images illustrating focal enrichment of eGFP-PCGF3 and eGFP-PCGF5 fusion proteins following induction of Xist RNA for 24 h (+dox) in *Suz12*$^{-/-}$ mESC. Focal enrichment is not seen in uninduced cells (-dox). Images are maximum intensity projections of six consecutive z-stacks. Scale bar is 10 µm. (B) Images illustrating focal enrichment of eGFP-PCGF3 and eGFP-PCGF5 fusion proteins following induction of ΔSX Xist for 24 h (+dox). Focal enrichment is not seen in cells expressing ΔXN Xist for 24 h (+dox). Images are maximum intensity projections of six consecutive z-stacks. Scale bar is 10 µm. (C) Immuno-FISH experiment for Xist RNA and GFP for cells expressing eGFP-PCGF3 and eGFP-PCGF5 after induction of ΔSX Xist or ΔXN Xist. Scale bar is 5 µm. Rep1 and Rep2 are biological replicates.

Fig S10

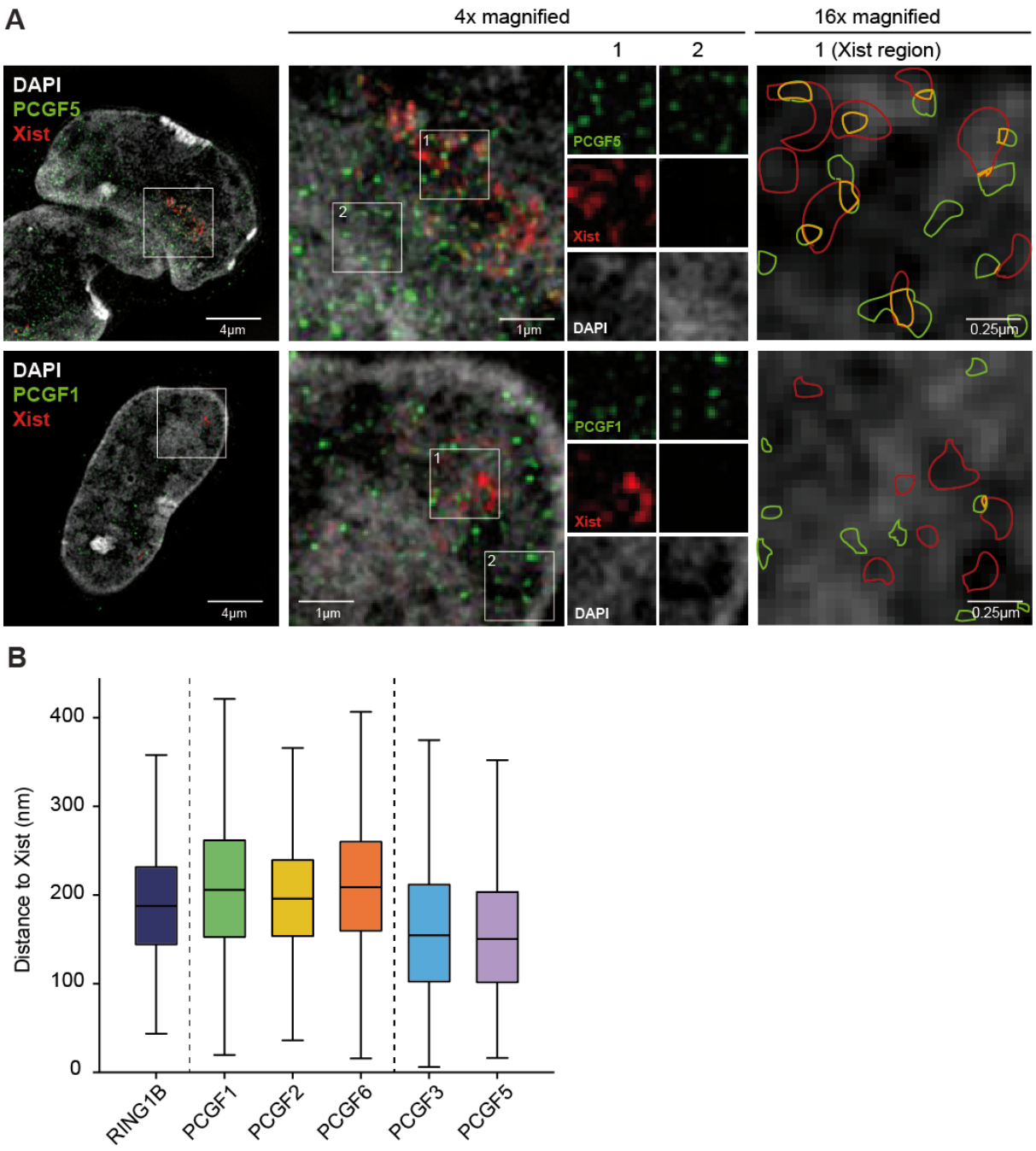

Fig. S10 3D-SIM analysis of eGFP-PCGF1, 2, 3, 5, 6 and RING1B relative to Xist RNA. (A) Examples illustrating 3D-SIM Immuno-FISH analysis of Xist RNA (red) and either eGFP-PCGF5 or eGFP-PCGF1 (green). The 4x magnified panels show the merged image. Insets 1 and 2 respectively correspond to the Xist domain and a randomly selected autosomal chromosome region. The 16x magnified panels illustrate the respective DAPI signal with outlined Xist (red), analysed protein (green), or co-localised signal (yellow). (B) Boxplot illustrating nearest neighbour/minimal distance analysis for each protein relative to Xist. eGFP-PCGF3 and eGFP-PCGF5 are significantly closer to Xist compared to other eGFP-PCGF proteins (Student t-test, $p<0.001$).

Fig S11

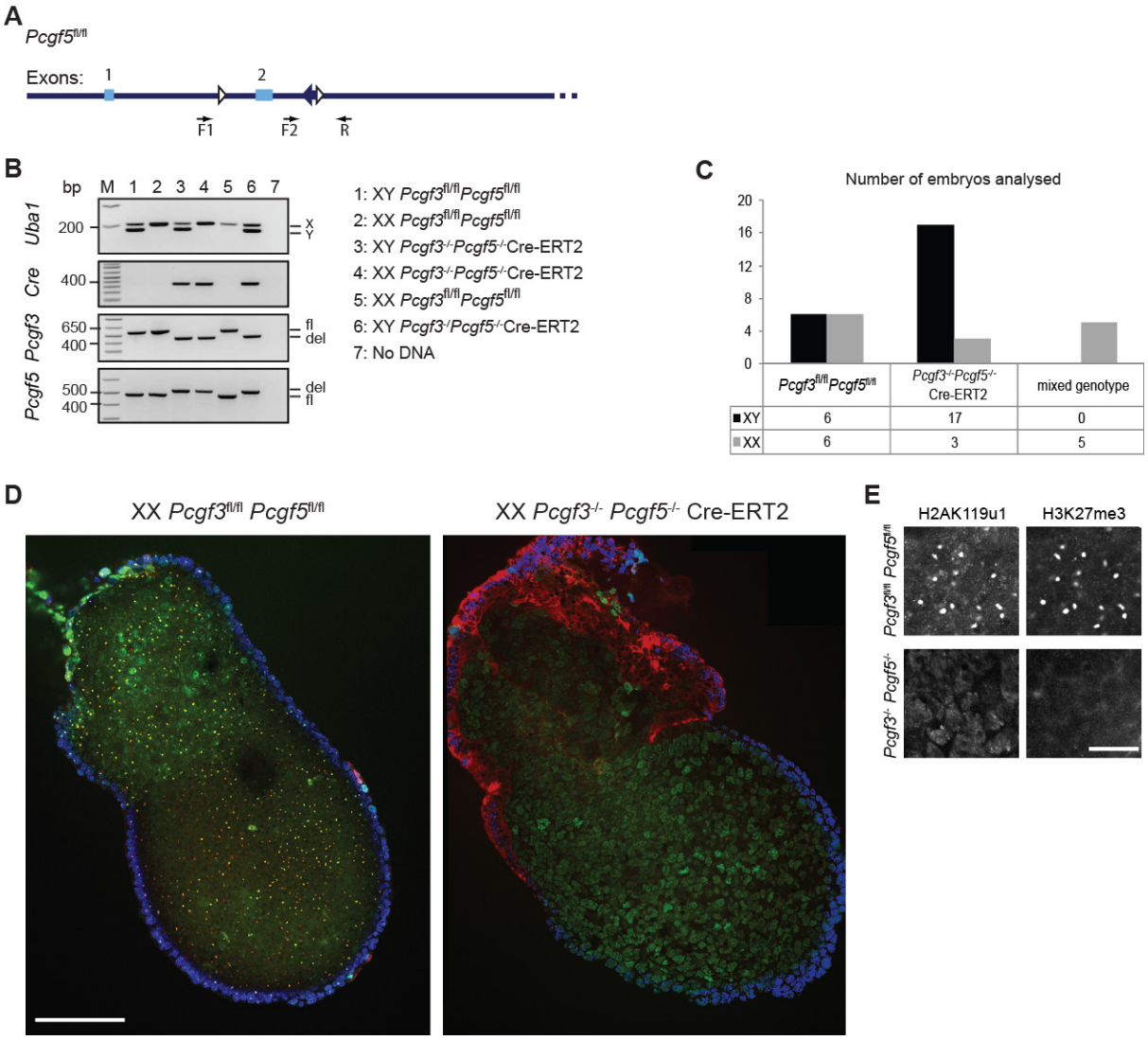

Fig. S11 Effect of Pcgf3/5 knockout in Polycomb recruitment by Xist RNA in vivo.
(A) Strategy for conditional null alleles of *Pcgf5* (*Pcgf5*$^{fl/fl}$). Schematics show intron/exon structure of the regions of interest with loxP (open triangles) and frt (filled triangle) site specific recombination recognition sites indicated. PCR primers used to discriminate floxed and deleted alleles are indicated (F1, F2 and R). (B) Genotyping of E7.5 embryos after immunofluorescence analysis. Representative examples are shown for *Uba1*, Cre-ERT2 (Cre), *Pcgf3* and *Pcgf5*. Pooled F1, F2 and R1 primers were used for both *Pcgf3* and *Pcgf5* genotyping. (C) Bar chart illustrating representation of different genotypes and the ratio of male and female E7.5 embryos recovered for immunofluorescence analysis after IVF, *in vitro* 4-hydroxytamoxifen treatment and transplantation into foster females. Mixed genotype column demonstrates the number of samples showing presence of *Pcgf5* deleted allele together with wt allele due to maternal tissue contamination. (D) Immunofluorescence analysis of H3K27me3 and H2AK119u1 domains in *Pcgf3/5* knockout female embryo and its floxed littermate at E7.5. Examples show tiled single focal plane confocal scans through the entire embryo (60x objective). Scale bar is 100 µm. (E) Immunofluorescence analysis of H2AK119u1 and H3K27me3 domains in *Pcgf3*$^{-/-}$:*Pcgf5*$^{-/-}$ and *Pcgf3*$^{fl/fl}$:*Pcgf5*$^{fl/fl}$ female embryos at E7.5. Images show representative single focal plane scans through extraembryonic region. Scale bar is 20 µm.

Fig S12

A

Pcgf3$^{+/-}$:*Pcgf5*$^{+/-}$ x *Pcgf3*$^{+/-}$:*Pcgf5*$^{+/-}$ → Dissect at E9.5/E10.5

Embryo ID	Stage	Sex	Embryo	Placenta
16-2	E9.5	♂	Yes	Yes
16-3		♀	No	Yes
16-5		♂	Yes	Yes
18-1		♀	No	Yes
19-10		♂	No	Yes
20-8		♂	Yes*	Yes
12-4		♂	Yes	Yes
23-1		♀	No	Yes
1-1	E10.5	♂	**	**
1-8		♀	**	**
11-4		♂	Yes*	Yes
14-1		♂	Yes*	Yes
16-1		♀	No	Yes

* Small embryo

** Resorbed conceptus

C

Genotype / Stage	*Pcgf3*$^{+/+}$ *Pcgf5*$^{+/+}$	*Pcgf3*$^{+/+}$ *Pcgf5*$^{+/-}$	*Pcgf3*$^{+/+}$ *Pcgf5*$^{-/-}$	*Pcgf3*$^{+/-}$ *Pcgf5*$^{+/+}$	*Pcgf3*$^{+/-}$ *Pcgf5*$^{+/-}$	*Pcgf3*$^{+/-}$ *Pcgf5*$^{-/-}$	*Pcgf3*$^{-/-}$ *Pcgf5*$^{+/+}$	*Pcgf3*$^{-/-}$ *Pcgf5*$^{+/-}$	*Pcgf3*$^{-/-}$ *Pcgf5*$^{-/-}$	Totals
E10.5♀	7	5	2	4	12	6	0	5	2	43
E10.5♂	2	4	0	2	3	1	2	9	3	26
Totals	9 (13.0)	9 (13.0)	2 (2.9)	6 (8.7)	15 (21.7)	7 (10.1)	2 (2.9)	14 (20.3)	5 (7.2)	69
E9.5♀	2	2	3	4	17	3	4	7	3	45
E9.5♂	1	4	0	2	9	3	3	2	5	29
Totals	3 (4.1)	6 (8.1)	3 (4.1)	6 (8.1)	26 (35.1)	6 (8.1)	7 (9.5)	9 (12.2)	8 (10.8)	74
Grand Totals	12 (8.4)	15 (10.5)	5 (3.5)	12 (8.4)	41 (28.7)	13 (9.1)	9 (6.3)	23 (16.1)	13 (9.1)	143

B

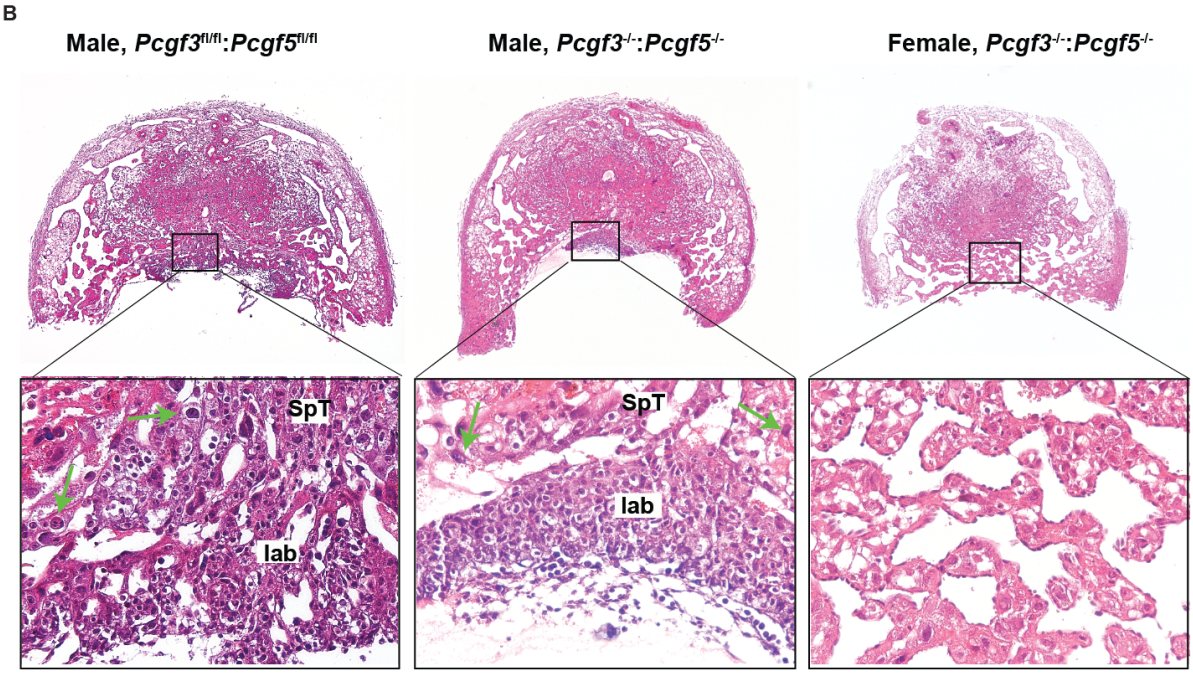

Fig. S12 Analysis of *Pcgf3/5* depletion effects in embryo development.

(A) Male and female Pcgf3/5 double knockout conceptuses obtained at E9.5 and E10.5. Recovery of a small embryo (*) or degraded conceptus (**) is indicated. (B) Examples illustrating cellular morphology in wild-type and *Pcgf3/5* double knockout male and female placentas determined by H&E staining of sections from paraffin embedded samples. Expanded view (boxed area) highlights key features: spongitrophoblast (SpT), labyrinth (lab) and trophoblast giant cells (arrows). (C) Data illustrating representation of different genotypes and ratios of males and females in embryos from *Pcgf3*$^{+/-}$: *Pcgf5*$^{+/-}$ heterozygote crosses at E9.5 and E10.5. Numbers in brackets show percentage representation of different genotypes.

Fig S13

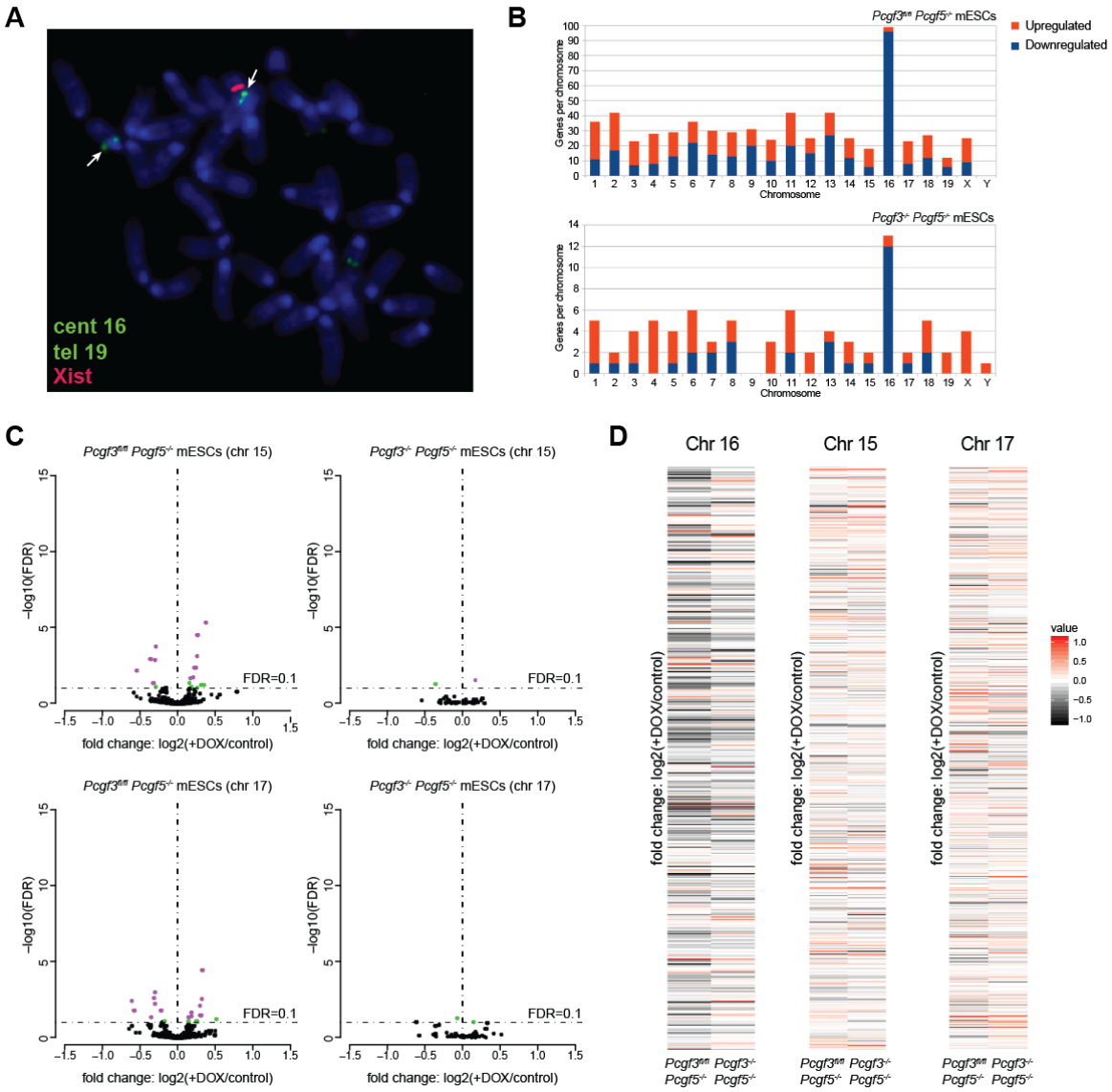

Fig. S13 Inducible Xist transgene integrated into single chromosome 16 downregulates genes located on this chromosome in *Pcgf3*$^{fl/fl}$ *Pcgf5*$^{-/-}$ and *Pcgf3*$^{-/-}$ *Pcgf5*$^{-/-}$ mESCs.

(A) FISH analysis of metaphase spreads showing integration of Xist transgene (red) into chromosome 16 (green, marked with arrows). Metaphase spreads were hybridized with a centromeric probe for chromosome 16 and a telomeric probe for chromosome 19 labeled with the same fluorophore (green) but easily discernible due to their localization in relation to the centromeres brightly labeled with DAPI. (B) Number of differentially expressed genes (FDR<0.1) per chromosome between Xist induced and control *Pcgf3*$^{fl/fl}$ *Pcgf5*$^{-/-}$ (top panel) and *Pcgf3*$^{-/-}$ *Pcgf5*$^{-/-}$ (bottom panel) mESCs. (C) Genes differentially expressed between Xist induced and control in *Pcgf3*$^{fl/fl}$ *Pcgf5*$^{-/-}$ (left panel) and *Pcgf3*$^{-/-}$ *Pcgf5*$^{-/-}$ (right panel) mESCs on chromosomes 15 (top panels) and 17 (bottom panel). Genes with FDR<0.05 are depicted in violet, FDR>0.05 and <0.1 are depicted in green. (D) Heatmaps showing expression changes between Xist induced and control for all expressed genes in *Pcgf3*$^{fl/fl}$ *Pcgf5*$^{-/-}$ and *Pcgf3*$^{-/-}$ *Pcgf5*$^{-/-}$ mESCs on chromosomes,16, where Xist is integrated, and other autosomes (chromosome 15 and 17).

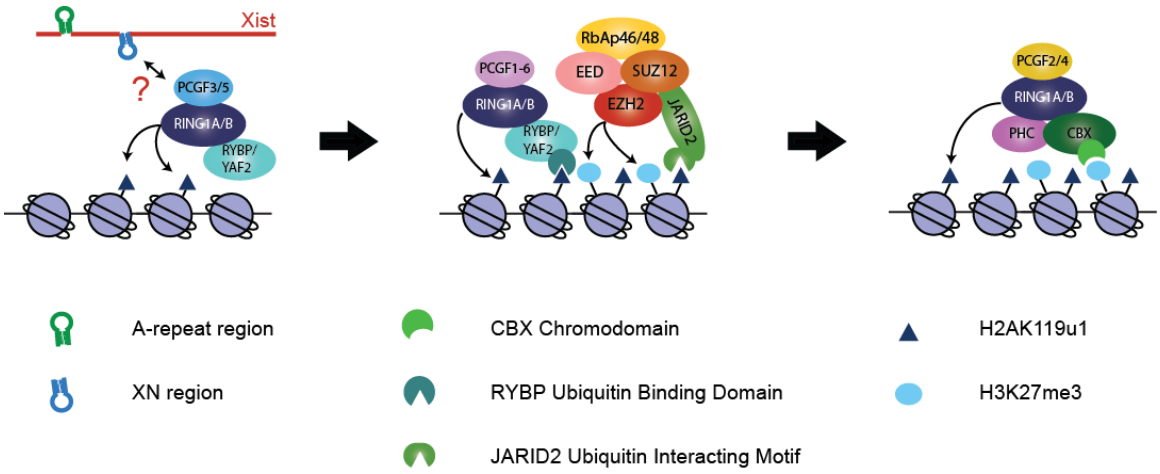

Fig. S14 Model summarizing key steps in Polycomb recruitment by Xist RNA. The model illustrated indicates that initiation of Polycomb recruitment involves interaction of PCGF3/5-PRC1 with the Xist XN region. It is currently unclear whether this interaction is direct or requires a co-factor. H2AK119u1 mediated by PCGF3/5-PRC1 serves to recruit other non-canonical PRC1 complexes through binding of the ubiquitin binding domain of the RYBP/YAF2 subunit, reinforcing H2AK119u1 deposition through positive feedback. Concomitantly, H2AK119u1 modified chromatin signals recruitment of PRC2, mediated at least in part by direct binding of the PRC2 cofactor JARID2, via a ubiquitin interacting motif. In a final step, PRC2 mediated H3K27me3 recruits canonical PRC1 complexes through interaction with the chromodomain of the PRC1 subunit CBX.

Movie S1: Live cell imaging of mouse ES cell line 3E-H expressing eGFP-PCGF proteins.

Movie S2: Live cell imaging of *Rybp*$^{-/-}$ *Yaf2*$^{-/-}$ mouse ES cell line expressing eGFP-PCGF1 upon Xist induction.

Movie S3: Live cell imaging of *Rybp*$^{-/-}$ *Yaf2*$^{-/-}$ mouse ES cell line expressing eGFP-PCGF2 upon Xist induction.

Movie S4: Live cell imaging of *Rybp*$^{-/-}$ *Yaf2*$^{-/-}$ mouse ES cell line expressing eGFP-PCGF3 upon Xist induction.

Movie S5: Live cell imaging of *Rybp*$^{-/-}$ *Yaf2*$^{-/-}$ mouse ES cell line expressing eGFP-PCGF5 upon Xist induction.

Movie S6: Live cell imaging of *Rybp*$^{-/-}$ *Yaf2*$^{-/-}$ mouse ES cell line expressing eGFP-PCGF6 upon Xist induction.

Additional Data Table S3 (separate file) List of genes differentially expressed between Xist induced (+dox) and control in *Pcgf3*$^{fl/fl}$ *Pcgf5*$^{-/-}$ mESCs (FDR<0.1).

Table contains list of differentially expressed genes along with FDR values, normalized read counts per gene and per 1kbp of the gene (mean from 4 replicates), together with fold change. The same values are provided for *Pcgf3*$^{-/-}$ *Pcgf5*$^{-/-}$ mESCs for comparison. These values were used to plot heatmap in Fig 4F.

References and Notes

1. Y. B. Schwartz, V. Pirrotta, A new world of Polycombs: Unexpected partnerships and emerging functions. *Nat. Rev. Genet.* **14**, 853–864 (2013). doi:10.1038/nrg3603 Medline

2. M. de Napoles, J. E. Mermoud, R. Wakao, Y. A. Tang, M. Endoh, R. Appanah, T. B. Nesterova, J. Silva, A. P. Otte, M. Vidal, H. Koseki, N. Brockdorff, Polycomb group proteins Ring1A/B link ubiquitylation of histone H2A to heritable gene silencing and X inactivation. *Dev. Cell* **7**, 663–676 (2004). doi:10.1016/j.devcel.2004.10.005 Medline

3. J. Silva, W. Mak, I. Zvetkova, R. Appanah, T. B. Nesterova, Z. Webster, A. H. Peters, T. Jenuwein, A. P. Otte, N. Brockdorff, Establishment of histone H3 methylation on the inactive X chromosome requires transient recruitment of Eed-Enx1 polycomb group complexes. *Dev. Cell* **4**, 481–495 (2003). doi:10.1016/S1534-5807(03)00068-6 Medline

4. K. Plath, J. Fang, S. K. Mlynarczyk-Evans, R. Cao, K. A. Worringer, H. Wang, C. C. de la Cruz, A. P. Otte, B. Panning, Y. Zhang, Role of histone H3 lysine 27 methylation in X inactivation. *Science* **300**, 131–135 (2003). doi:10.1126/science.1084274 Medline

5. J. Zhao, B. K. Sun, J. A. Erwin, J. J. Song, J. T. Lee, Polycomb proteins targeted by a short repeat RNA to the mouse X chromosome. *Science* **322**, 750–756 (2008). doi:10.1126/science.1163045 Medline

6. A. Cerase, D. Smeets, Y. A. Tang, M. Gdula, F. Kraus, M. Spivakov, B. Moindrot, M. Leleu, A. Tattermusch, J. Demmerle, T. B. Nesterova, C. Green, A. P. Otte, L. Schermelleh, N. Brockdorff, Spatial separation of Xist RNA and polycomb proteins revealed by superresolution microscopy. *Proc. Natl. Acad. Sci. U.S.A.* **111**, 2235–2240 (2014). doi:10.1073/pnas.1312951111 Medline

7. S. T. da Rocha, V. Boeva, M. Escamilla-Del-Arenal, K. Ancelin, C. Granier, N. R. Matias, S. Sanulli, J. Chow, E. Schulz, C. Picard, S. Kaneko, K. Helin, D. Reinberg, A. F. Stewart, A. Wutz, R. Margueron, E. Heard, Jarid2 is implicated in the initial Xist-induced targeting of PRC2 to the inactive X chromosome. *Mol. Cell* **53**, 301–316 (2014). doi:10.1016/j.molcel.2014.01.002 Medline

8. S. Schoeftner, A. K. Sengupta, S. Kubicek, K. Mechtler, L. Spahn, H. Koseki, T. Jenuwein, A. Wutz, Recruitment of PRC1 function at the initiation of X inactivation independent of PRC2 and silencing. *EMBO J.* **25**, 3110–3122 (2006). doi:10.1038/sj.emboj.7601187 Medline

9. L. Tavares, E. Dimitrova, D. Oxley, J. Webster, R. Poot, J. Demmers, K. Bezstarosti, S. Taylor, H. Ura, H. Koide, A. Wutz, M. Vidal, S. Elderkin, N. Brockdorff, RYBP-PRC1 complexes mediate H2A ubiquitylation at polycomb target sites independently of PRC2 and H3K27me3. *Cell* **148**, 664–678 (2012). doi:10.1016/j.cell.2011.12.029 Medline

10. C. Chu, Q. C. Zhang, S. T. da Rocha, R. A. Flynn, M. Bharadwaj, J. M. Calabrese, T. Magnuson, E. Heard, H. Y. Chang, Systematic discovery of Xist RNA binding proteins. *Cell* **161**, 404–416 (2015). doi:10.1016/j.cell.2015.03.025 Medline

11. N. P. Blackledge, A. M. Farcas, T. Kondo, H. W. King, J. F. McGouran, L. L. Hanssen, S. Ito, S. Cooper, K. Kondo, Y. Koseki, T. Ishikura, H. K. Long, T. W. Sheahan, N. Brockdorff, B. M. Kessler, H. Koseki, R. J. Klose, Variant PRC1 complex-dependent

H2A ubiquitylation drives PRC2 recruitment and polycomb domain formation. *Cell* **157**, 1445–1459 (2014). doi:10.1016/j.cell.2014.05.004 Medline

12. S. Cooper, M. Dienstbier, R. Hassan, L. Schermelleh, J. Sharif, N. P. Blackledge, V. De Marco, S. Elderkin, H. Koseki, R. Klose, A. Heger, N. Brockdorff, Targeting polycomb to pericentric heterochromatin in embryonic stem cells reveals a role for H2AK119u1 in PRC2 recruitment. *Cell Reports* **7**, 1456–1470 (2014). doi:10.1016/j.celrep.2014.04.012 Medline

13. R. Kalb, S. Latwiel, H. I. Baymaz, P. W. Jansen, C. W. Müller, M. Vermeulen, J. Müller, Histone H2A monoubiquitination promotes histone H3 methylation in Polycomb repression. *Nat. Struct. Mol. Biol.* **21**, 569–571 (2014). doi:10.1038/nsmb.2833 Medline

14. S. Cooper, A. Grijzenhout, E. Underwood, K. Ancelin, T. Zhang, T. B. Nesterova, B. Anil-Kirmizitas, A. Bassett, S. M. Kooistra, K. Agger, K. Helin, E. Heard, N. Brockdorff, Jarid2 binds mono-ubiquitylated H2A lysine 119 to mediate crosstalk between Polycomb complexes PRC1 and PRC2. *Nat. Commun.* **7**, 13661 (2016). doi:10.1038/ncomms13661 Medline

15. Materials and methods are available as supplementary materials.

16. Y. A. Tang, D. Huntley, G. Montana, A. Cerase, T. B. Nesterova, N. Brockdorff, Efficiency of Xist-mediated silencing on autosomes is linked to chromosomal domain organisation. *Epigenet. Chromatin* **3**, 10 (2010). doi:10.1186/1756-8935-3-10 Medline

17. Z. Gao, J. Zhang, R. Bonasio, F. Strino, A. Sawai, F. Parisi, Y. Kluger, D. Reinberg, PCGF homologs, CBX proteins, and RYBP define functionally distinct PRC1 family complexes. *Mol. Cell* **45**, 344–356 (2012). doi:10.1016/j.molcel.2012.01.002 Medline

18. B. Moindrot, A. Cerase, H. Coker, O. Masui, A. Grijzenhout, G. Pintacuda, L. Schermelleh, T. B. Nesterova, N. Brockdorff, A pooled shRNA screen identifies Rbm15, Spen, and Wtap as factors required for Xist RNA-mediated silencing. *Cell Reports* **12**, 562–572 (2015). doi:10.1016/j.celrep.2015.06.053 Medline

19. E. García, C. Marcos-Gutiérrez, M. del Mar Lorente, J. C. Moreno, M. Vidal, RYBP, a new repressor protein that interacts with components of the mammalian Polycomb complex, and with the transcription factor YY1. *EMBO J.* **18**, 3404–3418 (1999). doi:10.1093/emboj/18.12.3404 Medline

20. R. Arrigoni, S. L. Alam, J. A. Wamstad, V. J. Bardwell, W. I. Sundquist, N. Schreiber-Agus, The Polycomb-associated protein Rybp is a ubiquitin binding protein. *FEBS Lett.* **580**, 6233–6241 (2006). doi:10.1016/j.febslet.2006.10.027 Medline

21. J. Seibler, B. Zevnik, B. Küter-Luks, S. Andreas, H. Kern, T. Hennek, A. Rode, C. Heimann, N. Faust, G. Kauselmann, M. Schoor, R. Jaenisch, K. Rajewsky, R. Kühn, F. Schwenk, Rapid generation of inducible mouse mutants. *Nucleic Acids Res.* **31**, e12 (2003). doi:10.1093/nar/gng012 Medline

22. K. Sakai, Ji. Miyazaki, A transgenic mouse line that retains Cre recombinase activity in mature oocytes irrespective of the cre transgene transmission. *Biochem. Biophys. Res. Commun.* **237**, 318–324 (1997). doi:10.1006/bbrc.1997.7111 Medline

23. M. Endoh, T. A. Endo, T. Endoh, Y. Fujimura, O. Ohara, T. Toyoda, A. P. Otte, M. Okano, N. Brockdorff, M. Vidal, H. Koseki, Polycomb group proteins Ring1A/B are functionally linked to the core transcriptional regulatory circuitry to maintain ES cell identity. *Development* **135**, 1513–1524 (2008). doi:10.1242/dev.014340 Medline

24. F. A. Ran, P. D. Hsu, C. Y. Lin, J. S. Gootenberg, S. Konermann, A. E. Trevino, D. A. Scott, A. Inoue, S. Matoba, Y. Zhang, F. Zhang, Double nicking by RNA-guided CRISPR Cas9 for enhanced genome editing specificity. *Cell* **154**, 1380–1389 (2013). doi:10.1016/j.cell.2013.08.021 Medline

25. A. Wutz, T. P. Rasmussen, R. Jaenisch, Chromosomal silencing and localization are mediated by different domains of Xist RNA. *Nat. Genet.* **30**, 167–174 (2002). doi:10.1038/ng820 Medline

26. F. Mueller, T. S. Karpova, D. Mazza, J. G. McNally, Monitoring dynamic binding of chromatin proteins in vivo by fluorescence recovery after photobleaching. *Methods Mol. Biol.* **833**, 153–176 (2012). doi:10.1007/978-1-61779-477-3_11 Medline

27. B. L. Sprague, R. L. Pego, D. A. Stavreva, J. G. McNally, Analysis of binding reactions by fluorescence recovery after photobleaching. *Biophys. J.* **86**, 3473–3495 (2004). doi:10.1529/biophysj.103.026765 Medline

28. G. Ball, J. Demmerle, R. Kaufmann, I. Davis, I. M. Dobbie, L. Schermelleh, SIMcheck: A toolbox for successful super-resolution structured illumination microscopy. *Sci. Rep.* **5**, 15915 (2015). doi:10.1038/srep15915 Medline

29. J. D. Dignam, R. M. Lebovitz, R. G. Roeder, Accurate transcription initiation by RNA polymerase II in a soluble extract from isolated mammalian nuclei. *Nucleic Acids Res.* **11**, 1475–1489 (1983). doi:10.1093/nar/11.5.1475 Medline

30. T. Nojima, T. Gomes, A. R. Grosso, H. Kimura, M. J. Dye, S. Dhir, M. Carmo-Fonseca, N. J. Proudfoot, Mammalian NET-seq reveals genome-wide nascent transcription coupled to RNA processing. *Cell* **161**, 526–540 (2015). doi:10.1016/j.cell.2015.03.027 Medline

31. A. Dobin, C. A. Davis, F. Schlesinger, J. Drenkow, C. Zaleski, S. Jha, P. Batut, M. Chaisson, T. R. Gingeras, STAR: Ultrafast universal RNA-seq aligner. *Bioinformatics* **29**, 15–21 (2013). doi:10.1093/bioinformatics/bts635 Medline

32. W. Huber, V. J. Carey, R. Gentleman, S. Anders, M. Carlson, B. S. Carvalho, H. C. Bravo, S. Davis, L. Gatto, T. Girke, R. Gottardo, F. Hahne, K. D. Hansen, R. A. Irizarry, M. Lawrence, M. I. Love, J. MacDonald, V. Obenchain, A. K. Oleś, H. Pagès, A. Reyes, P. Shannon, G. K. Smyth, D. Tenenbaum, L. Waldron, M. Morgan, Orchestrating high-throughput genomic analysis with Bioconductor. *Nat. Methods* **12**, 115–121 (2015). doi:10.1038/nmeth.3252 Medline

33. L. Schmiedeberg, P. Skene, A. Deaton, A. Bird, A temporal threshold for formaldehyde crosslinking and fixation. *PLOS ONE* **4**, e4636 (2009). doi:10.1371/journal.pone.0004636 Medline

34. D. Smeets, Y. Markaki, V. J. Schmid, F. Kraus, A. Tattermusch, A. Cerase, M. Sterr, S. Fiedler, J. Demmerle, J. Popken, H. Leonhardt, N. Brockdorff, T. Cremer, L. Schermelleh, M. Cremer, Three-dimensional super-resolution microscopy of the inactive X chromosome territory reveals a collapse of its active nuclear compartment harboring

distinct Xist RNA foci. *Epigenetics Chromatin* **7**, 8 (2014). doi:10.1186/1756-8935-7-8 Medline